arXiv:astro-ph/0106474v1 26 Jun 2001

Difference Image Analysis of the OGLE-II bulge data. II. Microlensing events.

P.R. Woźniak[1,2], A. Udalski[3], M. Szymański[3], M. Kubiak[3], G. Pietrzyński[3,4], I. Soszyński[3], K. Żebruń[3]

[1] *Princeton University Observatory, Princeton, NJ 08544, USA*

[2] *Los Alamos National Laboratory, MS-D436, Los Alamos, NM 87545, USA*

e-mail: wozniak@lanl.gov

[3] *Warsaw University Observatory, Al. Ujazdowskie 4, 00-478 Warszawa, Poland*

e-mail: (udalski,msz,mk,pietrzyn,soszynsk,zebrun)@astrouw.edu.pl

[4] *Universidad de Concepción, Departamento de Fisica, Casilla, 160-C, Concepción, Chile*

e-mail: pietrzyn@hubble.cfm.udec.cl

ABSTRACT

We present a sample of microlensing events discovered in the Difference Image Analysis (DIA) of the OGLE-II images collected during 3 observing seasons, 1997–1999. 4424 light curves pass our criteria on the presence of a brightening episode on top of a constant baseline. Among those, 512 candidate microlensing events were selected visually. We designed an automated procedure, which unambiguously selects up to 237 best events. Including 8 candidate events recovered by other means, a total of 520 light curves are presented in this work.

In addition to microlensing events, the larger sample contains certain types of transients, but is also strongly contaminated by artifacts. All 4424 light curves in the weakly filtered group are available electronically, with the intent of showing the gray zone between microlensing events and variable stars, as well as artifacts, to some extent inevitable in massive data reductions. We welcome suggestions for improving the selection process before the full analysis of complete 4 seasons of the OGLE-II bulge data. Selection criteria for binary events can also be investigated with our extended sample.

1. Introduction

Microlensing, and its potential to probe the mass distribution of compact dark objects in the Galaxy, were first proposed as an observational subject in mid eighties (Paczyński 1986). Since the first discoveries in 1993 Galactic microlensing has grown into a whole new field of astrophysics with several teams conducting large monitoring programs of the densest stellar fields of the sky (see Paczyński 1996 for a review). The cross section to detectable light magnification by a stellar mass lens in the Galaxy is of the order 10^{-6} in case of typical sources in the Milky Way bulge, and 10^{-7} for sources in LMC and SMC. If we want to maintain practical event rates, this leads to monitoring millions of stars over extended time intervals. The main goal of these efforts still remains unchanged: to provide large samples of microlensing events with the best possible understanding of involved systematics. The line of sight towards the Galactic bar returns most events, and several estimates of the optical depth based on conventional PSF photometry are already available. Early estimates came from OGLE-I (9 events, Udalski et al. 1994a) and MACHO (45 events, Alcock et al. 1997), and both gave a somewhat unexpectedly large value $\sim 3.5 \times 10^{-6}$ with 30–50% uncertainty. Popowski et al. (2000) emphasized that the available information is insufficient for a robust comparison with models. Only continued effort can improve this situation. Their optical depth of $(2.0 \pm 0.5) \times 10^{-6}$, based on 52 events with red clump giants as sources, should be less prone to blending and partially alleviates the problem.

Measuring the mass spectrum of lenses will most likely require individual mass estimates using interferometric follow up (possibly from space) of the most promising events, for which the degeneracy between physical lens parameters can be broken (Gould 1995 and references therein). Nevertheless, with photometry alone for about 1500 well covered events with good signal to noise and well assessed blending, one could normalize model components of the inner galaxy by comparing corresponding maps of predicted optical depth with the observed number of events across the Galactic bar (Han & Gould 1995).

The Optical Gravitational Lensing Experiment, after its upgrade to OGLE-II in 1997, collected data with the new, dedicated 1.3 m Warsaw Telescope at the Las Campanas Observatory. OGLE-II database contains 4 seasons of data, a total of 15,500 I band images in 49 bulge fields covering 11 square degrees. The Early Warning System (Udalski et al. 1994b), adapted to OGLE-II, reached the rate of 78 events per year discovered in real time during the observing season of 2000 and posted on the OGLE web page at *http://www.astrouw.edu.pl/∼ftp/ogle/ogle2/ews/ews.html*. A catalog of 214 events from the off line search of 3 years of data was published by Udalski et al. (2000). Presently OGLE has upgraded its 2k×2k pixel camera to a mosaic of 8 2k×4k CCDs. By scaling the number of detections, we can expect up to 1000 events per year from OGLE-III, starting in mid 2001.

Limitations associated with photometry in extremely crowded fields stimulated the development of difference imaging techniques, specifically their adaptations for microlensing. Currently, two algorithms have successful large applications: Fourier division (Tomaney & Crotts 1996, Alcock et al. 1999a) and linear kernel decomposition in real space (Alard & Lupton 1998, Alard 2000, Woźniak 2000, and more recently Bond et al. 2001). Difference Image Analysis (DIA) offers numerous advantages over conventional PSF photometry for variable objects in crowded environments. After matching PSFs of two images of the same stellar field, the difference flux corresponding to these images is no longer crowded. There is no need for fitting multi-PSF models, which is usually a degenerate procedure and results in strongly non-Gaussian error distributions. In fields as crowded as the Galactic bulge, typically several stars contribute light to a single observed PSF. DIA removes biases in the light centroid of the variable star. It also provides generally much better S/N ratio, which results in more detections. Alcock et al. (2000b) obtained a supposedly less biased value of the optical depth in Baade's Window using DIA: $(3.2 \pm 0.5) \times 10^{-6}$, in better than just formal agreement with the early work. However, they analyzed only 8 out of 94 MACHO fields.

In this paper we present a sample of microlensing events discovered in a complete reanalysis of 3 seasons of the OGLE-II bulge data using DIA photometry based on the algorithm of Alard & Lupton (1998) and Alard (2000). Our main purpose is to eliminate human judgment, and design a fully automatic selection procedure, which has not been accomplished in OGLE-II so far (Udalski et al. 2000). In Section 4 we present a programmable algorithm, which unambiguously selects events best interpreted as microlensing upon visual inspection. This step is essential in determination of the efficiency function to detection of microlensing events, a necessary ingredient of the optical depth estimates. Additionally, we discuss a possible source of contamination of the OGLE-II and other microlensing samples, the existence of artifact light curves. With the released sample of light curves, the confusion between microlensing, variability of other kinds and instrumental artifacts can be studied. Such training data can also be used to refine classifiers of single microlensing events and, even more interestingly, to attack the problem of automated selection of binary and other exotic events.

2. Data

All OGLE-II frames were collected with the 1.3 m Warsaw Telescope at the Las Campanas Observatory, Chile. The observatory is operated by the Carnegie Institution of Washington. The "first generation" OGLE camera uses a SITe 3 2048×2048 CCD detector

with 24μm pixels resulting in 0.417″ pixel^{-1} scale. Images of the Galactic bulge are taken in driftscan mode at "medium" readout speed with the gain 7.1 e^-/ADU and readout noise of 6.3 e^-. Saturation level is about 55,000 ADU. For the details of the instrumental setup, we refer the reader to Udalski, Kubiak & Szymański (1997).

The majority of frames was taken in the I photometric band. Effective exposure time is 87 seconds. During observing seasons of 1997–1999 the OGLE experiment collected typically between 200 and 300 I-band frames for each of the 49 bulge fields BUL_SC1–49. OGLE-II images are 2k×8k strips, corresponding to $14' \times 57'$ in the sky, therefore the total covered area of the bulge is about 11 square degrees. The number of frames in V and B bands is small and we do not analyze them with the DIA method. The median seeing is 1.3″ for our data set. In Table 1 we provide equatorial and galactic coordinates of the field centers and the total number of analyzed frames. Figure 1 schematically shows locations of the OGLE-II bulge fields with respect to the Galactic bar. Fields BUL_SC45 and BUL_SC46 were observed much less frequently, mostly with the purpose of maintaining phases of variable stars discovered by OGLE-I. Observations of fields BUL_SC47–49 started in 1998; the season of 1997 is not available for them.

3. DIA photometry of OGLE-II bulge frames

The DIA data pipeline we used is based on the image subtraction algorithm developed by Alard & Lupton (1998) and Alard (2000), and was written by Woźniak (2000). Processing of large 2k×8k pixel frames is done after division into 512×128 pixel subframes with 14 pixel margin to ensure smooth transitions between coordinate transformations and fits to spatially variable PSF for individual pieces. Small subframe size allows us to use polynomial fits for drift scan images, in which PSF shape and local coordinate system vary on scales of 100–200 pixels. The reference image, subtracted from all images of any given field, is a stack of 20 best images in the sequence.

We adopted kernel expansion used by Woźniak (2000), generally applicable to all OGLE-II data. The kernel model, represented by a 15×15 pixel raster, consists of 3 Gaussians with sigmas 0.78, 1.35, and 2.34 pixels, multiplied by polynomials of orders 4, 3, and 2 respectively. The pipeline delivers a list of candidate variable objects and their difference light curves. The initial filtering is very weak, with only minimum of assumptions about the variability type. Candidate variables are flagged as "transient" or "continuous" variables depending on whether variability is confined to episodes in an otherwise quiet object, or spread throughout the observed time interval. The total number of candidate variables in all 49 fields was slightly over 220,000, including 150,000 "continuous" and 66,000 "transient"

cases. Only 4600 objects passed both filters, confirming sensible definitions of classes. This initial classification is refined in Section 4.1. Number of detected variable objects in a given field depends on the number density of stars, extinction, and number of available measurements. It ranged from about 800 to over 9000 per field. Variability database for all 49 fields comprises 2 GB of data.

The error distribution in measurements from our DIA pipeline is nearly Gaussian with the average scatter only 17% above the Poisson limit for faint stars near I=17–19 mag, gradually increasing for brighter stars, and reaching 2.5 times photon noise at $I \sim 11$ mag (about 0.5% of the total flux). Error bars adopted in this paper are photon noise estimates renormalized using the curve of Woźniak (2000). Because the method effectively monitors all pixels for possible variability, microlensing events may be discovered even where no object is detected in the reference image. In regular searches monitoring is conducted only for objects detected in a single good quality image, a template. This issue is related to centroid finding. Currently in our DIA pipeline centroids are calculated based on the variable signal in a number of frames. As a result the centroid will be poorly known for an object with low S/N variability, even if it is very bright on the reference image. Ideally one would use both pieces of information. It is usually obvious how to determine the centroid in the presence of blending when confronted with one particular object of interest, but an optimal algorithm for extracting all variability in the field using DIA is yet to be developed.

4. Search for events

Microlensing event selection algorithms of leading surveys are very involved, multi-step procedures with numerous vaguely justified fudge factors. The underlying problem is that the error distributions in photometry are usually not Gaussian and poorly controlled. In the MACHO project several levels of cuts aim solely at filtering known types of variable stars, and the χ^2 statistic based on formal error bars is weighted with the event amplitude (see Alcock et al. 2000b for criteria with the DIA photometry). EROS team came up with the algorithm, in which short period variables are rejected based on large deviations of points from linear interpolation between the two neighboring measurements (e.g. Afonso et al. 1999). Both teams make use of color information and approximate achromaticity of microlensing. Simultaneous observations with more than one filter provide a strong veto against artifacts. Dwarf novae are sufficiently blue during outbursts to be rejected based on their colors (Alcock et al. 1999b). Unfortunately the number of the OGLE-II observations in V and B bands is very small compared to I, and cuts based on achromaticity are out of the question.

Woźniak (2000) made a preliminary statement that using the DIA method 512 microlensing events were found in 3 observing seasons of data for all 49 OGLE bulge fields. 305 of those were recovered in an algorithmic search. At the time, however, the detailed noise properties of the sample were not known and the old algorithm was fairly artificial. In particular, the properties of the Gaussian distribution of errors were not explicitly used. We abandon this approach and develop an entirely new set of criteria with less emphasis on the number of events, more attention to reducing the number of involved parameters, and better suited for approximately Gaussian noise in our DIA photometry.

In the early days of OGLE-I A. Udalski was the first to fully appreciate that one of the important variability characteristics of microlensing events is that most of the time there is no variability at all. The main selection criterion for microlensing in OGLE requires that the star is formally constant during at least one observing season and varies only within a localized time interval (Udalski et al. 1994a). Despite the fact that this cut shortens the list of candidate light curves by a large factor, so far the final selection of events in OGLE-II still involved visual inspection of many candidates (Udalski et al. 2000). In this work we attempted to define selection cuts which grasp the main idea of a long constant baseline, but also exploit good noise properties of the DIA measurements allowing a better use of χ^2 related statistics.

4.1. Transients

Before the main selection process, light curves are cleaned of suspicious points. Occasional problems with bleeding columns and undetected cosmic rays produce points with irrelevant values, which can be spotted using several parameters supplied by the pipeline. First, we remove points which came from poor difference frames with χ^2 per pixel above 6.0. Measurements with 4 or more saturated pixels within the fitting radius are also removed. Next, we determine the median photometric error of all remaining measurements and median χ^2 per pixel value of the corresponding PSF fits. We reject the points for which either the photometric error or χ^2 per pixel is a factor of 10 larger than the median. Usually almost all measurements are admitted, nevertheless these filters are necessary to prevent loss of good events due to a few bad points. Finally, we reject stars with centroids determined using fewer than 4 frames and the total number of useful measurements below 50% of all frames for a given field. This removes numerous stars very close to one of the frame edges.

In the next step, we check for the presence of a constant baseline in the light curve. We define a running window of length equal to 50% of all usable measurements, and select the position of the window which minimizes $\sigma_{F_{\rm base}}$, the scatter around the mean $F_{\rm base}$. In order

to avoid discrimination against both ends of the observed period, it is assumed that after the last point the light curve continues starting over from the beginning. To check for possible variability in the baseline we bin the window into 10 point intervals and calculate the mean F and σ_F in each bin separately. We require that all but maximum 2 individual means stay within $\sigma_{F_{\rm base}}$ of $F_{\rm base}$. Also the mean of individual σ_F values in all bins cannot be lower than $0.5\sigma_{F_{\rm base}}$, to exclude smooth, long term variability within the baseline.

We also define a dynamic threshold for interesting brightening episodes. If $N_{0-1\sigma}$ is the number of points within $1\sigma_{F_{\rm base}}$ of $F_{\rm base}$, and $N_{1-3\sigma}$ the number of points between 1 and 3 $\sigma_{F_{\rm base}}$ of $F_{\rm base}$, the expected ratio $N_{1-3\sigma}/N_{0-1\sigma}$ is about 32/68 for a Gaussian distribution. Larger ratios suggest the presence of non-Gaussian wings, which may result from intrinsic variability of the source. If $\sigma_{\rm ph}$ is the mean photometric error estimate for points in the baseline window, the ratio $\sigma_{F_{\rm base}}/\sigma_{\rm ph}$ should be near 1 in the absence of variability. Intrinsic variability or atypically crowded environment could result in larger values. At this stage we admit low amplitude variables with brightening episodes and leave the margin for some scatter around the average baseline properties by increasing the threshold.

We adopt threshold δ:

$$\delta \;=\; \sigma_{F_{\rm base}} \times \delta_1 \times \delta_2, \tag{1}$$

where

$$\delta_1 \;=\; \max\left\{\frac{N_{1-3\sigma}/N_{0-1\sigma}}{32/68}, 1\right\} \tag{2}$$

$$\delta_2 \;=\; \max\left\{\frac{\sigma_{F_{\rm base}}}{\sigma_{\rm ph}}, 1\right\} \tag{3}$$

The limit $\sigma_{F_{\rm base}}/\sigma_{\rm ph} < 2.5$ is set on the allowed scatter in the baseline for all objects flagged initially by the pipeline as "transient" type (Section 3 and Woźniak (2000)). Candidate variables flagged as "continuous" do not enter the main study and are treated separately (Section 4.2).

Once the presence of a constant baseline is established, we look for brightening episodes in the light curve using threshold δ. We declare that there is an episode if N consecutive points deviate by nδ up or down with respect to $F_{\rm base}$. We consider two types of episodes with (N, nδ) values of (3, 5δ) and (4, 4δ). It is required that the candidate transient event has 1 or 2 separate episodes above the baseline flux within at least one of the above types. No

episodes below the baseline flux are allowed. The last requirement removes some interesting variables, which may be a subject of a separate study.

A total of 4424 light curves went through these cuts, roughly 2% of the group initially suspected of variability. Most of them have episodes with very few points at low signal to noise, and therefore very poorly known centroids. Another numerous type which escapes filtering is very slow and low signal to noise trend. Some of those could be due to proper motions just at the limit of detection (Eyer & Woźniak 2000). Instrumental artifacts are a serious problem in all microlensing searches due to the amount of data which has to be filtered for each discovered event. This topic is usually ignored in papers. We find that real stellar variability background is easier to separate from microlensing than artifacts, which account for most of our 4424 "transients". A group of candidate variables with close positions on the frame and similar looking light curves is a clear indication of a problem. Unfortunately the wings of very bright, saturated stars can generate ghost variables within many tenths of pixels due to changing weather conditions and their own variability. Nevertheless, the final list of "transients" contains many interesting objects, including microlensing events. We conclude that prior knowledge about the type of variability is essential for effective searches. In particular, microlensing model fits are critical for an automated detection of events in the presence of contaminating background of artifacts.

4.2. Microlensing events

To make sure that we include binary lensing events and other interesting departures from classic single point mass microlensing, a visual search through light curves from the previous cut is performed first. We made fits of the single microlensing curve for all 4424 candidates from Section 4.1. The model in the form:

$$M(t) = F_0 + F_1 \times (A(t) - 1), \tag{4}$$

where

$$A(t) = \frac{u^2 + 2}{u\sqrt{u^2 + 4}} \tag{5}$$

$$u^2 = u_0^2 + \left(\frac{t - t_{\max}}{t_0}\right)^2, \tag{6}$$

includes the unknown zero point F_0 in addition to the lensed flux F_1, the impact parameter u_0, the Einstein ring crossing time t_0, and the moment of maximum $t_{\rm max}$. By visual comparison with the fit, we recovered 512 light curves, for which the best interpretation is microlensing.

Then, we defined several parameters of the fit, and in the so constructed parameter space we examined the locus of our visually selected sample compared to the remaining episodic light curves. Our efforts to quantify what makes observers believe that they are seeing microlensing resulted in the following conclusion: in addition to a well defined baseline, the next important property is the presence of several consecutive high S/N points which are well fitted with the microlensing curve. Therefore, the main parameter distinguishing single microlensing events from other types of variability in our search is:

$$R = \max_k \left[\frac{\sum_{i=k}^{k+11} (f_i - F_0)^2}{\sum_{i=k}^{k+11} (f_i - M_i)^2} \right]^{1/2} , \qquad (7)$$

where f_i is the flux of the i-th observation, F_0 is the fitted baseline flux, M_i is the best fit microlensing model, the sums are over a 12 point window, and R is the maximum value of the ratio over the entire light curve. In case of a good fit R is roughly proportional to S/N ratio, while for a bad fit R is much lower, even in cases of high S/N variability. Again, we formally run the test on cyclic light curves with the beginning and the end joined together.

As emphasized before, in microlensing light curve one expects a baseline which is long compared to the event duration. The use of total χ^2 or total χ^2/d.o.f. is not very efficient in this case. It is important to have a handle on the goodness of fit separately near the event and far from the event, in the baseline. We define the event region of the light curve, where the flux from the best fit model is at least 1 median error $d_{1/2}$ above F_0. We calculate two approximately χ^2 distributed sums:

$$s_1 = \frac{1}{(m_1 - 4)} \sum_{M_i - F_0 > d_{1/2}} \frac{(f_i - M_i)^2}{\sigma_i^2} \qquad (8)$$

for m_1 points in the event region and

$$s_2 = \frac{1}{(m_2 - 1)} \sum_{M_i - F_0 < d_{1/2}} \frac{(f_i - M_i)^2}{\sigma_i^2} \qquad (9)$$

for m_2 points of the baseline region, both of which should stay near 1 for normal cases of microlensing and properly normalized errors. We also consider total duration of the event T, the time between the beginning and the end of the event region, as given by the best fit model. Long lasting events are ambiguous, because their baselines are short relative to the duration of the experiment. This notion can be quantified by setting a higher S/N threshold for longer events.

In Figure 2 we show the distribution in the (s_1, R) plane of candidate light curves with $s_2 < 2.0$, and $0 < T < 500$ days, and minimum 8 high points in the event region. A high point is simply the one detected at more than 3σ above the baseline. Single microlensing events are relatively well separated by R alone, with all remaining types of variability and artifacts located at low R and spanning a large range in s_1. Above $R = 15$ there are no light curves of unwanted types, and there are 134 events with reasonably good fits, that is $s_1 < 2.0$. It is possible to decrease the limit on signal to noise to $R = 10$ for shorter events with $T < 200$ days, as shown in Figure 3. This relaxed cut selects 188 events.

The above criteria strongly reject events with any departures from a single point mass microlensing model. In Figures 2 and 3 some events from the visual sample are located in the region of $R < 10$ and have poor fits with $s_1 > 3.0$. These are mostly cases of binary lensing and possibly binary sources. Other departures from a perfect fit to the model are expected too. The cumulative error distribution in Woźniak (2000) revealed a weak non-Gaussian tail at the level of $\sim 1\%$. Outlying points can also be produced by parallactic effects and weakly binary events with very low mass companions, like Jovian planets. Examples of possible planetary disturbances include: SC20 1793, SC29 2054, SC36 7980, and SC39 3160. In the present sample their nature can only be studied statistically. A direct detection will require much more frequent observations, which are planned for some of the fields in OGLE-III. Such events should be included in the determination of the optical depth. Therefore, we perform iterative procedure, in which we reject the worst point in the fit, obtain a new fit and reexamine all parameters of the event. There are 237 events which pass the above defined criteria after between 0 and 5 consecutively worst points are removed. All light curves selected in this way were also selected visually. We show these best events in Figure **??**. Figure **??** shows light curves of the remaining candidate events selected visually from the group which passed the criteria in Section 4.1. For those, the uncertainty of classification is generally larger. The corresponding model fits and some basic data are presented in Tables 2 and 3. Columns are: 1. OGLE field number, 2. star number in the DIA variability database, 3. star number in the OGLE database for events cross identified with the OGLE catalog of events, 4. 5. equatorial coordinates, 6. base line difference flux, 7. lensed flux, 8. impact parameter, 9. Einstein ring crossing time, 10. moment of maximum light (JD Hel.-2450000), 11. base line I magnitude, 12. f, the ratio of the lensed flux to the total base line flux.

Columns 6.–10. are best fit model parameters. Columns 11.–12. are derived from 6.–7. using calibration data distributed with light curves (Section 5). The fits are preliminary in a sense that the near degeneracy of the microlensing curve occasionally results in unphysical values of the best fit parameters. In such cases a careful study using additional information is usually needed in order to find a better model.

We correlated positions of the candidate variables in our DIA data with the positions of 214 microlensing events reported by Udalski et al. (2000). The nearest candidate within a 2 pixel radius ($0.8''$) was adopted as a positive identification. 127 events out of 237 in our algorithmic sample were identified, 39 more positive matches came out of the visual sample. In the process we recovered 8 additional events from the DIA variability data (Table 4 and Figure **??**). Three of them actually passed the criteria for "transients" (Section 4.1) but have not been picked up visually: BUL_SC3 7783, SC5 4321 and SC37 8176. Three more events failed the test for a constant base line because of their extremely long duration, and two remaining ones had the base line scatter above the limits. SC44 1980 seems to be a genuine variable which went through a microlensing event. OGLE database identifications for 174 events are included in Tables 2, 3 and 4. This leaves us with 40 events reported by Udalski et al. (2000) which did not make it to the initial list of suspected variables. Most of these light curves have peaks with very low S/N ratio, however 6 events in this group were well measured by the standard OGLE photometric pipeline. One of the selection cuts for candidate variables in the DIA pipeline is based on how well the PSF fits the residual in the so called variability image (Woźniak 2000). Most likely, the parameters of this cut need some adjustment. As mentioned before, the optimal algorithm for extracting variability from difference images is still a subject of research.

Selection of binary microlensing events has never been automated. Some of the binary events pass the algorithmic criteria adopted by the MACHO team, but the presence of a strong second peak is used by MACHO to reject events (Alcock et al. 2000b). Binary fraction among all events from the MACHO Alert System (Alcock et al. 2000a) and visually selected samples from OGLE (Udalski et al. 2000), roughly agree with what is known about binary stars (Mao & Paczyński 1991). However, there are unexpectedly few reports of weak binaries without caustic crossings compared to predictions of Di Stefano (2000), suggesting a strong bias towards low impact parameters and a connection to blending (Alcock et al. 2000a). In particular, our sample does not include a single light curve, which consists of two well separated point mass microlensing peaks. Such events should occur due to lensing by wide binary systems, in which the separation between the two components is several times larger than both Einstein ring radii. Our sample of 4424 light curves provides some testing ground for a more systematic study.

5. Discussion and future work

We demonstrated that the process of selecting microlensing events in OGLE-II data can be automated with the use of the DIA photometry. In summary, the main steps of the automated selection of microlensing events are: identification of the constant baseline, detecting an event region in the light curve with several high signal to noise points, and finally, adjusting the threshold on S/N for the longest (and therefore more ambiguous) events. Elimination of human judgment in this procedure will allow a reliable determination of detection efficiencies, and ultimately optical depth to microlensing. In addition to the data for microlensing events found in this analysis, the full set of light curves which passed much weaker constraints on variability type (Section 4.1), is available electronically at *http://www.astro.princeton.edu/∼wozniak/dia/lens*. README file provides full details on light curves, calibration data and other information which could not fit in this paper. We encourage individuals to work with our weakly filtered data on better selection criteria for single and binary microlensing events. We also believe that it is important to show the gray zone of microlensing surveys, where the background of variable stars, and even more problematic background of artifacts, has to be separated from the actual events.

Extremely large volumes of data processed by microlensing surveys are very likely to hide interesting surprises. In case of the DIA analysis of the OGLE-II BUL_SC1 field, the strategy of releasing samples selected using relaxed criteria has already paid off with the photometric discovery of proper motions in very dense stellar fields (Eyer & Woźniak 2000). Presently released set of microlensing events has a much better controlled error distribution than the standard DoPhot output, which makes it suitable for setting an upper limit on the number of Jupiter mass planets around lensing stars.

The set of the OGLE-II images is closed. In the course of this project, the last, fourth season of data was collected. All available images will be reprocessed in the near future using pipeline of Woźniak (2000). We plan to adopt stricter approach to badly saturated stars by rejecting larger areas around them. The cost of up to 10% loss of the survey area is still acceptable, as the intermediate samples of variable objects will be much less contaminated by spurious variability. In the mean time, we expect the final calibration of the OGLE-II database of standard PSF photometry from the DoPhot based pipeline to be completed. DIA light curves will be converted to standard Johnson–Cousins filters. Difference imaging technique is being considered as the primary mode of data reduction in OGLE-III, which started collecting new images in mid 2001 using a mosaic of 8 2k×4k CCDs. Still frame images of OGLE-III will undoubtedly have much weaker spatial PSF variations and should be easier to handle with the DIA photometry.

We would like to thank Prof. Paczyński for constant support and numerous insightful discussions. This work was supported by the NSF grant AST-9820314 to Bohdan Paczyński, Polish KBN grant 2P03D00814 to A. Udalski, and 2P03D00916 to M. Szymański. Additional support was provided by the Laboratory Directed Research & Development funds (X1EM and XARF programs at LANL).

REFERENCES

Afonso, C., et al., 1999, A&A, 344, L63

Alard, C., & Lupton, R. H., 1998, ApJ 503, 325

Alard, C., 2000, A&AS, 144, 363

Alcock, C., et al., 1997, ApJ, 479, 119

Alcock, C., et al., 1999a, ApJ, 521, 602

Alcock, C., et al., 1999b, ApJS, 124, 171

Alcock, C., et al., 2000a, ApJ, 541, 270

Alcock, C., et al., 2000b, ApJ, 541, 734

Bond, I. A., et al., 2001, MNRAS, submitted, astro-ph/0102184

Di Stefano, R., 2000, ApJ, 541, 587

Eyer, L., & Woźniak, P., 2001, MNRAS, in press, astro-ph/0102027

Gould, A., 1995, ApJ, 441, L21

Han, C., & Gould, A., 1995, ApJ, 449, 521

Mao, S., & Paczyński, B., 1991, ApJ, 374, L37

Paczyński, B., 1986, ApJ, 304, 1

Paczyński, B., 1996, ARA&A, 34, 419

Popowski, P., et al., 2000, ASP Conf. Series, in press, Microlensing 2000: A New Era of Microlensing Astrophysics, ed. J.W. Menzies and P.D. Sackett, astro-ph/0005466

Tomaney, A. B., & Crotts, A. P., 1996, AJ, 112, 2872

Udalski, A., Szymański, M., Stanek, K. Z., Kałużny, J., Kubiak, M., Mateo, M., Krzeminski, W., Paczyński, B., & Venkat, R., 1994a, Acta Astron., 44, 165

Udalski, A., Szymański, M., Kałużny, J., Kubiak, M., Mateo, M., Krzemiński, W., Paczyński, B., 1994b, Acta Astron., 44, 227

Udalski, A., Kubiak, M., & Szymański, M., 1997, Acta Astron., 47, 319

Udalski, A., Żebruń, K., Szymański, M., Kubiak, M., Pietrzyński, G. Soszyński, I., Woźniak, P. R., 2000, Acta Astron., 50, 1

Woźniak, P. R., 2000, Acta Astron., 50, 421, astro-ph/0012143

This preprint was prepared with the AAS LaTeX macros v5.0.

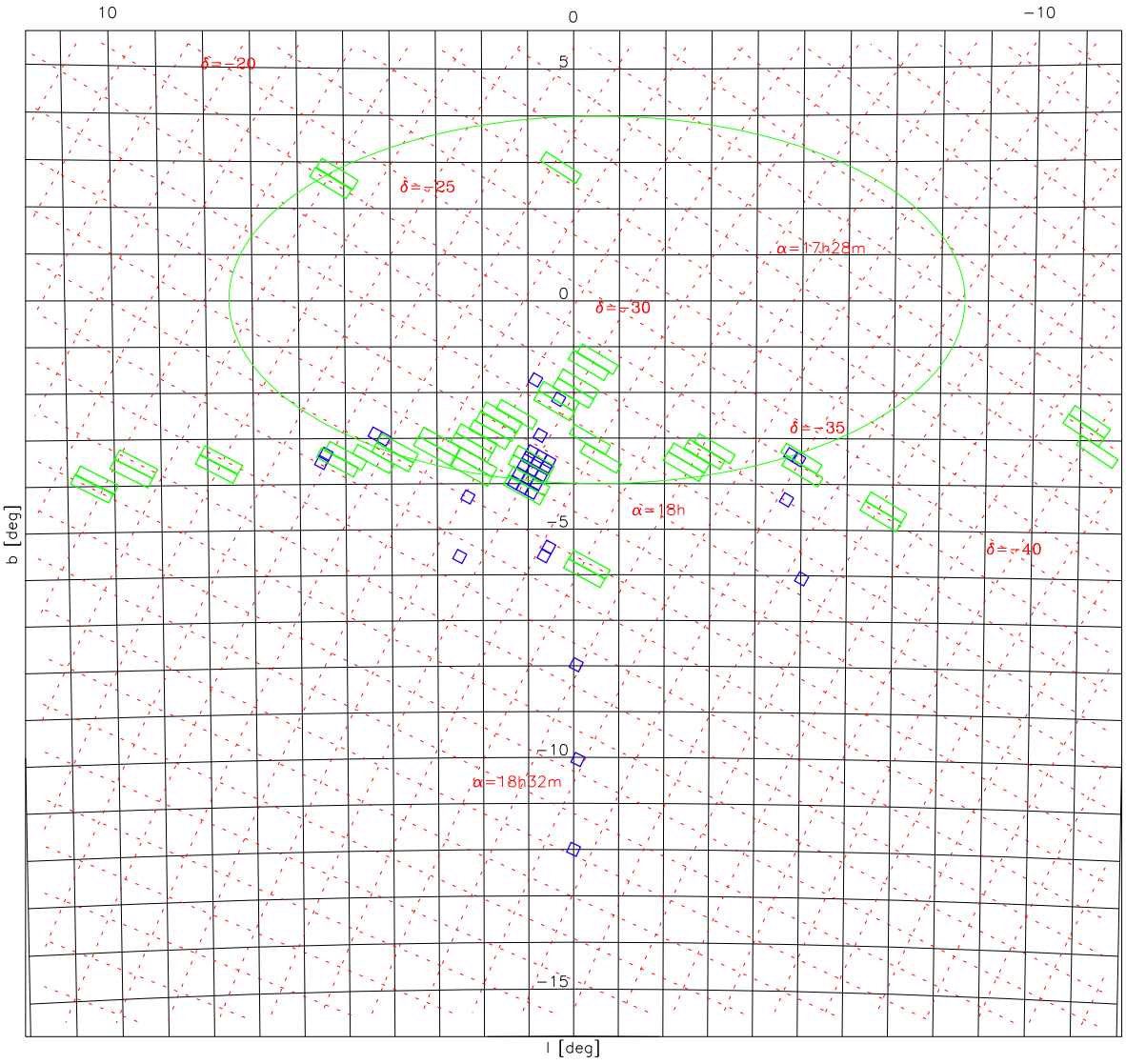

Fig. 1.— OGLE bulge fields in galactic coordinates (gnomonic projection, great circles are mapped to straight lines). Green strips are the OGLE-II scans and blue squares are the old OGLE-I fields. Large oval indicates the location of the Galactic bar. Fields are selected in windows of low extinction and avoid very bright foreground stars.

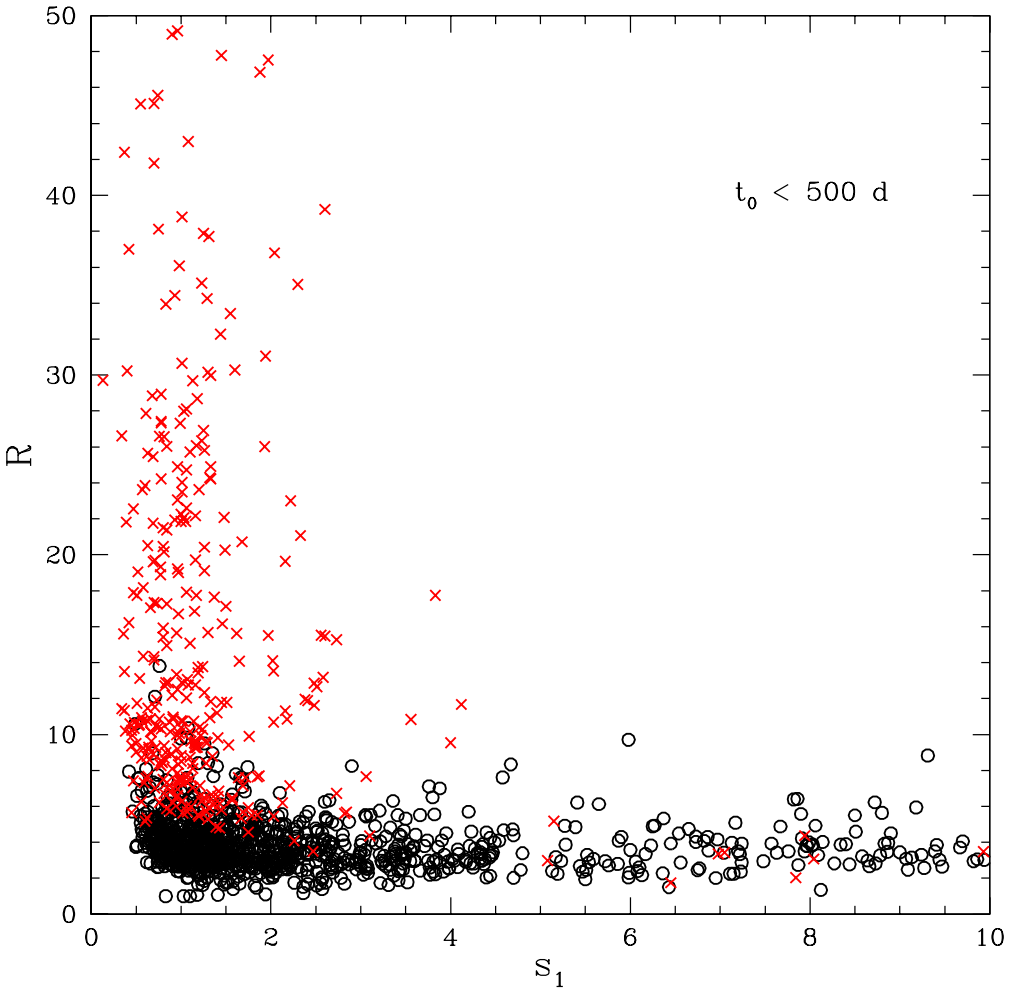

Fig. 2.— Distribution in the (s_1, R) plane of microlensing events (red crosses) visually selected among the light curves which passed the automated selection criteria for "transients" (black circles). DIA photometry allowed a great reduction of the region where microlensing events can be easily confused with other effects.

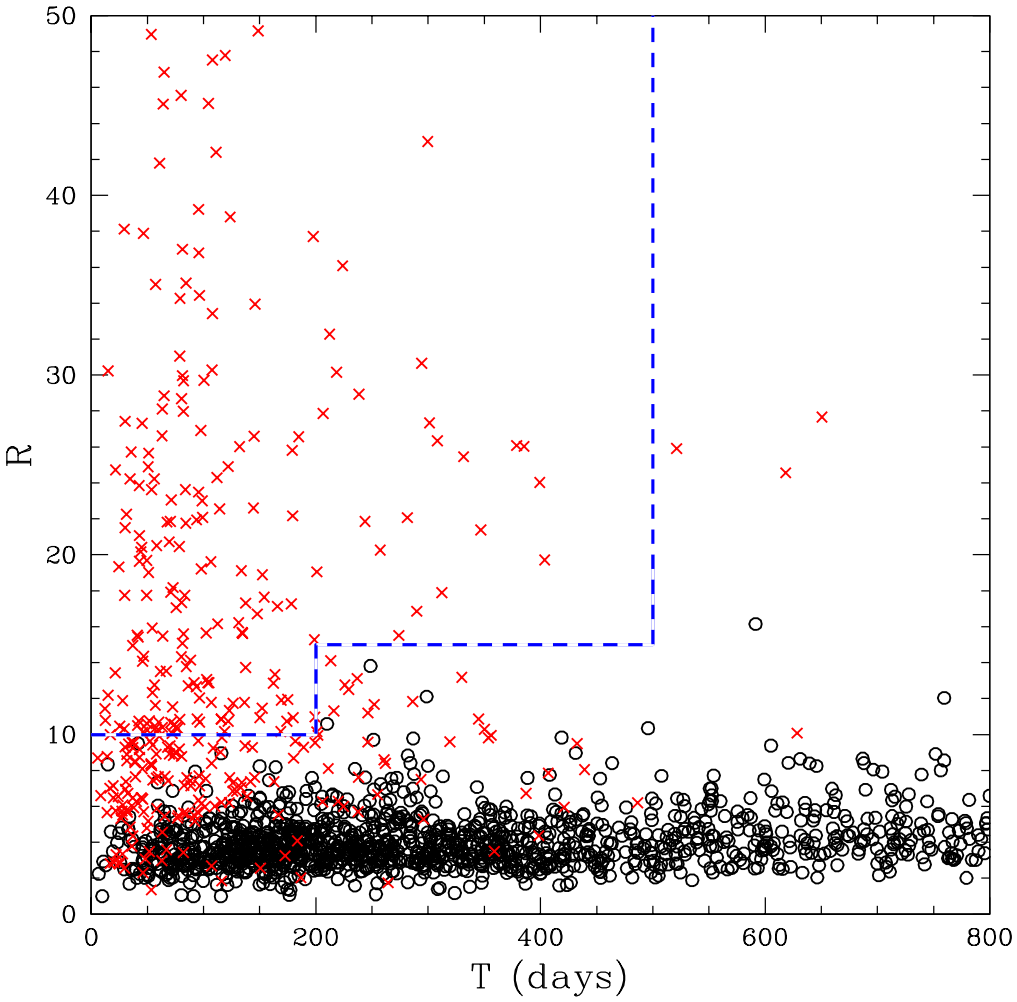

Fig. 3.— Distribution of visually selected microlensing events (red crosses) and automatically selected "transient" light curves (black circles) in the (T, R) plane. Selection based on R alone (S/N ratio and goodness of fit) becomes more uncertain for events with long durations T. The blue dashed line corresponds to the final selection cut adopted in Section 4.2.

Table 1. OGLE-II bulge fields.

Field	α_{2000} h m s	δ_{2000} ° ′ ″	l °	b °	$N_{\rm obs}$
BUL_SC1	18:02:32.5	−29:57:41	1.08	−3.62	197
BUL_SC2	18:04:28.6	−28:52:35	2.23	−3.46	192
BUL_SC3	17:53:34.4	−29:57:56	0.11	−1.93	309
BUL_SC4	17:54:35.7	−29:43:41	0.43	−2.01	324
BUL_SC5	17:50:21.7	−29:56:49	−0.23	−1.33	307
BUL_SC6	18:08:03.7	−32:07:48	−0.25	−5.70	228
BUL_SC7	18:09:05.5	−32:07:10	−0.14	−5.91	219
BUL_SC8	18:23:06.2	−21:47:53	10.48	−3.78	211
BUL_SC9	18:24:00.0	−21:47:10	10.59	−3.98	212
BUL_SC10	18:20:06.6	−22:23:03	9.64	−3.44	220
BUL_SC11	18:21:06.5	−22:23:05	9.74	−3.64	215
BUL_SC12	18:16:06.3	−23:57:54	7.80	−3.37	209
BUL_SC13	18:17:02.6	−23:57:44	7.91	−3.58	208
BUL_SC14	17:47:02.7	−23:07:30	5.23	2.81	209
BUL_SC15	17:48:06.9	−23:06:09	5.38	2.63	204
BUL_SC16	18:10:06.7	−26:18:05	5.10	−3.29	202
BUL_SC17	18:11:03.6	−26:12:35	5.28	−3.45	200
BUL_SC18	18:07:03.5	−27:12:48	3.97	−3.14	203
BUL_SC19	18:08:02.4	−27:12:45	4.08	−3.35	195
BUL_SC20	17:59:16.0	−28:52:10	1.68	−2.47	235
BUL_SC21	18:00:22.3	−28:51:45	1.80	−2.66	238
BUL_SC22	17:56:47.6	−30:47:46	−0.26	−2.95	275
BUL_SC23	17:57:54.5	−31:12:36	−0.50	−3.36	255
BUL_SC24	17:53:17.9	−32:52:45	−2.44	−3.36	250
BUL_SC25	17:54:21.0	−32:52:10	−2.32	−3.56	243
BUL_SC26	17:47:15.5	−34:59:31	−4.90	−3.37	241
BUL_SC27	17:48:23.6	−35:09:32	−4.92	−3.65	220
BUL_SC28	17:47:00.0	−37:07:10	−6.76	−4.42	217
BUL_SC29	17:48:10.8	−37:07:21	−6.64	−4.62	211
BUL_SC30	18:01:25.0	−28:49:55	1.94	−2.84	233

Table 1—Continued

Field	α_{2000} h m s	δ_{2000} ° ′ ″	l °	b °	$N_{\rm obs}$
BUL_SC31	18:02:22.6	−28:37:21	2.23	−2.94	236
BUL_SC32	18:03:24.0	−28:37:10	2.34	−3.14	231
BUL_SC33	18:05:30.9	−28:52:50	2.35	−3.66	187
BUL_SC34	17:58:18.5	−29:07:50	1.35	−2.40	239
BUL_SC35	18:04:28.6	−27:56:56	3.05	−3.00	177
BUL_SC36	18:05:31.2	−27:56:44	3.16	−3.20	209
BUL_SC37	17:52:32.2	−29:57:44	0.00	−1.74	305
BUL_SC38	18:01:28.0	−29:57:01	0.97	−3.42	191
BUL_SC39	17:55:39.1	−29:44:52	0.53	−2.21	318
BUL_SC40	17:51:06.1	−33:15:11	−2.99	−3.14	205
BUL_SC41	17:52:07.2	−33:07:41	−2.78	−3.27	208
BUL_SC42	18:09:05.0	−26:51:53	4.48	−3.38	204
BUL_SC43	17:35:10.0	−27:10:10	0.37	2.95	251
BUL_SC44	17:49:22.4	−30:02:45	−0.43	−1.19	258
BUL_SC45	18:03:33.0	−30:05:00	0.98	−3.94	88
BUL_SC46	18:04:36.0	−30:05:00	1.09	−4.14	84
BUL_SC47	17:27:00.0	−39:46:00	−11.19	−2.60	151
BUL_SC48	17:28:10.0	−39:46:00	−11.07	−2.78	145
BUL_SC49	17:29:20.0	−40:16:00	−11.36	−3.25	142

Table 2. Microlensing events found in the algorithmic search. See Section 4.2 for details.

Field	Star		α_{2000}	δ_{2000}	F_0	F_1	u_0	t_0	$t_{\max}$	I_0	f
	DIA	OGLE									
sc1	1943		18:02:11.82	-30:00:58.2	-16.8	85.0	0.3437	24.55	1323.47	17.130	0.287
sc1	2186		18:02:44.87	-29:58:18.2	0.7	38.3	0.3650	17.25	989.99	19.078	0.769
sc2	854	27414	18:04:04.92	-29:11:38.4	-16.1	208.1	0.5183	8.22	562.32	18.145	1.724
sc2	1799	65831	18:04:06.84	-29:01:17.1	-104.2	601.2	0.3559	58.34	1457.29	14.580	0.197
sc2	2017	495787	18:04:42.37	-28:59:38.8	-0.3	20.8	0.1338	38.52	1082.80	18.504	0.235
sc2	3095		18:03:58.77	-28:47:39.3	-24.4	18.6	0.0214	43.37	1411.39	20.204	1.102
sc2	3191		18:04:26.22	-28:46:49.4	-2.6	33.0	0.2390	19.76	583.10	19.427	0.899
sc2	4003		18:04:38.59	-28:38:39.6	6.2	183.9	0.2990	16.51	931.29	17.301	0.687
sc2	4310		18:04:39.00	-28:35:19.4	-40.1	1253.1	1.2692	20.46	560.43	16.387	2.132
sc2	5062		18:04:58.85	-28:27:04.3	-11.4	60.2	0.2478	15.88	597.42	18.355	0.616
sc3	655		17:53:05.25	-30:20:36.2	-0.1	10.7	0.0922	8.59	573.93	18.605	0.135
sc3	1427	457512	17:53:41.47	-30:14:54.0	-8.7	346.3	1.1613	14.53	1320.67	17.263	1.284
sc3	1514		17:53:19.54	-30:14:27.2	-2.3	50.1	0.2485	15.54	1057.33	19.293	1.162
sc3	1752		17:53:28.47	-30:12:11.9	-7.0	6.4	0.1069	58.58	1318.59	18.159	0.052
sc3	2030	469296	17:53:40.36	-30:10:20.2	0.6	282.0	0.3128	37.60	887.63	17.216	0.993
sc3	2379	480386	17:53:41.54	-30:08:12.7	-13.8	157.4	0.5291	9.36	611.65	17.799	0.930
sc3	2931		17:53:50.00	-30:04:34.7	1.3	32.7	0.1299	7.83	574.86	18.287	0.306
sc3	3136	77887	17:53:09.83	-30:02:52.4	-39.4	30.8	0.1429	87.89	1365.56	17.187	0.104
sc3	3369	91382	17:53:09.33	-30:01:12.1	1.8	553.2	0.0796	37.46	956.02	16.494	1.067
sc3	3975		17:53:50.54	-29:57:25.8	-1.3	50.2	0.5365	23.78	693.12	18.499	0.561
sc3	5453	541151	17:53:47.52	-29:47:48.5	1.7	99.3	0.1870	35.23	690.43	17.923	0.664
sc3	5474		17:53:53.21	-29:47:59.1	-7.3	0.4	0.0103	388.26	1405.62	20.112	0.019
sc3	5508		17:53:09.61	-29:46:39.5	-86.8	3110.4	1.6751	17.29	1409.00	14.930	1.284
sc3	5697		17:53:33.93	-29:46:15.6	-28.3	1820.2	0.7758	36.20	1477.20	15.692	1.531
sc3	6118		17:53:31.57	-29:43:06.1	0.1	51.9	0.7040	8.65	563.28	17.996	0.371
sc3	6344		17:54:03.43	-29:42:43.5	-1.5	11.7	0.1208	12.70	601.82	18.175	0.098
sc3	6597		17:53:43.04	-29:40:28.8	-5.9	187.6	0.9279	17.00	628.47	17.670	0.967
sc3	6913		17:53:39.88	-29:39:12.0	-2.1	62.5	0.8738	22.20	627.89	19.504	1.759
sc3	6914	576464	17:53:41.56	-29:39:06.1	-8.3	475.7	0.5173	36.61	656.21	16.215	0.647
sc3	7390	792295	17:53:54.14	-29:36:40.8	-26.9	136.5	0.3051	55.60	1054.68	19.461	3.696
sc3	7895	588309	17:53:38.65	-29:33:42.3	-51.1	2737.9	1.2832	23.98	1049.21	14.886	1.076
sc3	8335	601945	17:53:36.63	-29:31:21.3	2.4	227.5	0.6903	41.50	923.56	17.310	0.881
sc4	462	411329	17:54:43.66	-30:08:31.7	-13.7	6.6	0.0162	35.74	667.25	18.197	0.059
sc4	1903	631094	17:54:58.79	-30:00:11.9	-15.8	18.8	0.1331	49.37	1036.31	18.471	0.221
sc4	2612	451457	17:54:44.69	-29:55:42.8	-3.6	411.2	0.0248	36.48	1129.66	16.780	0.925
sc4	2843	267762	17:54:21.79	-29:53:24.0	0.8	1198.3	0.2215	7.42	971.10	15.477	0.858
sc4	3178	273327	17:54:19.52	-29:51:49.8	-29.0	184.0	0.2905	6.02	648.17	18.203	1.591
sc4	3392	463924	17:54:43.93	-29:51:18.2	-37.9	555.5	0.9233	29.00	1061.53	16.536	1.036
sc4	3503		17:54:22.59	-29:49:56.6	-5.1	66.8	0.1252	26.64	1311.71	17.498	0.299
sc4	4983		17:54:22.89	-29:42:11.4	-4.3	1.2	0.0048	393.02	1371.70	17.628	0.006
sc4	5611		17:54:34.09	-29:39:10.1	-4.3	25.2	0.1584	23.95	1438.69	17.944	0.173
sc4	5775		17:54:28.33	-29:38:02.3	0.4	11.8	0.0488	25.97	1323.54	17.709	0.066
sc4	6154	134300	17:54:13.04	-29:35:14.2	-40.1	11.3	0.0526	148.22	1040.87	16.725	0.025
sc4	6450	522952	17:54:38.64	-29:33:12.8	-1.3	1428.0	0.4284	24.35	1257.19	15.402	0.954
sc4	8412	568740	17:54:49.35	-29:20:25.0	3.7	314.8	0.3482	29.04	915.46	15.597	0.256
sc4	8607	201173	17:54:15.98	-29:18:49.6	-0.9	18.5	0.1079	28.25	1318.71	18.547	0.220
sc5	691		17:50:49.32	-30:18:56.2	-6.8	17.2	0.0953	11.48	563.86	17.323	0.067
sc5	3299	372272	17:50:42.72	-29:58:13.7	-13.9	1378.1	1.3887	15.16	617.73	15.526	1.061

Table 2—Continued

Field	Star		α_{2000}	δ_{2000}	F_0	F_1	u_0	t_0	$t_{\max}$	I_0	f
	DIA	OGLE									
sc5	4515	59256	17:49:55.59	-29:48:03.2	-21.2	65.2	0.2751	12.02	1043.27	18.716	0.914
sc5	4858	63662	17:49:52.76	-29:45:27.3	-1.6	178.2	0.4672	14.13	934.62	17.772	1.056
sc5	4862		17:50:03.61	-29:45:44.2	-0.3	10.7	0.1814	37.42	1304.20	19.916	0.459
sc6	2563	243857	18:08:02.64	-31:49:05.2	-47.9	134.5	0.0750	89.50	1251.97	17.728	0.787
sc8	171		18:22:55.93	-22:10:23.2	-7.4	1.0	0.0041	190.35	1291.69	21.658	0.219
sc10	1233	294229	18:20:20.61	-22:24:10.1	-9.6	65.5	0.2168	32.62	625.59	18.888	1.027
sc10	1809		18:19:48.84	-22:11:22.3	3.5	61.7	0.6693	30.20	709.30	18.975	1.128
sc10	2438	454300	18:20:30.00	-21:57:04.8	-72.5	286.9	0.0725	22.30	1391.88	17.594	1.525
sc13	23	148843	18:16:53.05	-24:25:47.3	-17.6	15.6	0.0953	168.16	1436.84	17.926	0.114
sc13	755		18:17:01.24	-24:11:53.9	-7.5	8.1	0.1336	65.21	568.39	20.381	0.574
sc14	423	480480	17:47:26.02	-23:30:03.5	-29.6	584.1	0.9764	12.48	575.07	16.560	1.123
sc14	674		17:46:44.53	-23:25:15.0	-1.0	45.5	0.4975	14.07	652.01	19.132	0.935
sc14	802	194722	17:46:47.64	-23:24:02.0	0.1	1128.3	1.6205	13.31	996.68	15.998	1.246
sc14	2433		17:47:14.45	-23:01:49.4	5.3	24.9	0.2116	31.24	1393.12	15.353	0.015
sc14	2612		17:47:27.51	-23:00:50.8	-10.7	66.5	0.8392	36.21	1359.01	18.811	1.045
sc14	4009	463284	17:47:02.94	-22:40:26.3	-11.3	292.3	1.4806	30.12	591.50	18.898	4.977
sc15	167	165930	17:48:01.11	-23:31:36.5	-1.3	163.4	0.7439	11.29	665.32	17.949	1.059
sc15	914	345180	17:48:13.79	-23:20:38.1	-77.7	1362.6	1.3495	35.71	603.60	15.492	1.017
sc15	1962		17:47:59.19	-23:07:46.4	-2.6	4.2	0.0593	42.84	1320.57	18.579	0.047
sc15	2154	530219	17:48:29.60	-23:04:54.7	-4.6	472.9	0.6528	89.90	936.45	14.968	0.218
sc15	2424	539556	17:48:27.68	-23:00:11.8	-4.7	1236.2	0.8924	30.22	665.60	16.084	1.478
sc15	2887	418332	17:48:08.12	-22:53:12.6	-21.2	119.8	0.8386	58.25	1358.75	17.965	0.803
sc15	2962		17:47:45.26	-22:51:12.5	-27.1	7469.1	1.7449	20.14	679.45	14.104	1.352
sc16	2161	436041	18:10:10.17	-26:21:03.2	-25.6	125.2	0.2406	65.77	540.02	18.388	1.227
sc18	118	2397	18:06:34.59	-27:39:51.4	-34.8	173.8	0.2318	18.31	626.51	18.135	1.361
sc18	498	596044	18:07:23.54	-27:36:18.7	-12.2	93.4	0.4651	17.17	1364.46	18.873	1.498
sc18	641	594723	18:07:20.85	-27:34:10.7	-7.3	39.2	0.0012	29.97	943.80	18.581	0.485
sc18	1134	242825	18:06:54.83	-27:29:21.7	-0.6	192.6	0.8290	26.58	995.41	17.626	0.918
sc18	2491	81415	18:06:37.15	-27:16:27.0	-10.6	600.0	1.4727	7.65	1358.74	18.344	5.699
sc19	1813		18:07:34.69	-27:20:44.0	-3.5	2.1	0.0198	111.91	1295.44	20.656	0.170
sc19	2209		18:08:13.35	-27:18:00.9	-0.0	15.8	0.0905	46.20	667.67	19.897	0.616
sc19	3181		18:08:19.60	-27:05:54.8	-3.8	11.5	0.1598	57.15	645.48	19.630	0.377
sc19	4350		18:07:51.01	-26:53:40.7	-6.8	56.6	0.7646	63.71	639.30	18.704	0.722
sc20	1742		17:59:24.45	-29:04:20.6	-6.5	134.5	0.0552	11.18	1386.06	17.971	0.873
sc20	1793		17:59:02.69	-29:03:03.0	-2.8	1776.3	1.3542	6.59	617.93	15.377	1.097
sc20	2596	300548	17:59:15.87	-28:55:49.6	-8.2	210.4	0.6365	44.06	1071.03	18.234	1.678
sc20	2674	305095	17:59:07.75	-28:54:41.2	-9.2	114.1	0.5197	10.50	1365.18	19.045	1.992
sc20	3525	708586	17:59:41.15	-28:47:18.5	-70.1	19.7	0.0310	52.08	1343.98	18.570	0.226
sc20	5032		17:58:54.32	-28:32:54.0	-3.2	13.9	0.1381	38.78	596.85	19.081	0.267
sc20	5174	560821	17:59:27.20	-28:32:31.5	-10.9	3037.6	1.0530	14.80	1052.53	14.789	1.123
sc20	5451	391296	17:59:17.01	-28:29:42.1	-5.3	32.4	0.1260	51.69	963.95	19.210	0.708
sc20	5748		17:59:39.05	-28:27:16.6	-25.4	1.8	0.0068	742.39	1276.29	18.471	0.021
sc21	97	678389	18:00:40.22	-29:19:34.9	-2.4	51.3	0.1271	92.41	894.32	18.051	0.386
sc21	424		18:00:14.06	-29:16:02.4	-34.8	40.3	0.1397	20.82	1339.95	19.351	1.072
sc21	1334		18:00:36.39	-29:09:46.3	-7.2	9.6	0.0529	74.43	1424.72	18.319	0.093
sc21	1395		17:59:53.39	-29:09:07.8	-9.8	4348.8	0.0155	27.03	500.43	15.369	2.872
sc21	3182		17:59:55.83	-28:55:44.7	0.3	56.6	0.3063	6.55	566.36	18.581	0.670
sc21	3381	766993	18:00:39.38	-28:55:14.6	-1.4	406.9	0.4354	55.32	1129.73	15.469	0.284

Table 2—Continued

Field	Star		α_{2000}	δ_{2000}	F_0	F_1	u_0	t_0	$t_{\max}$	I_0	f
	DIA	OGLE									
sc21	3388		18:00:50.21	-28:55:01.5	0.1	76.3	0.3310	29.38	983.29	17.337	0.297
sc21	4129		18:00:45.25	-28:49:36.5	-1.4	3.0	0.0160	181.26	988.95	19.205	0.065
sc21	4300		18:00:00.30	-28:47:57.9	-0.8	996.6	1.7571	12.15	1012.21	17.517	4.981
sc21	4826	388360	18:00:06.73	-28:44:00.5	1.9	24.0	0.0480	30.71	957.74	18.741	0.338
sc21	5554		18:00:19.54	-28:38:41.2	-1.2	7.6	0.1137	89.89	697.39	19.320	0.183
sc21	5954		18:00:30.03	-28:35:53.2	-18.2	8.7	0.0503	56.67	1312.31	18.905	0.144
sc22	173	383717	17:56:58.81	-31:14:06.5	-20.0	64.2	0.1742	24.32	588.16	19.241	1.514
sc22	337	390560	17:56:56.81	-31:11:51.0	-6.2	884.7	0.7023	14.66	1074.37	16.359	1.362
sc22	428	392070	17:56:52.98	-31:10:56.2	-13.6	34.0	0.2408	22.73	1043.03	17.881	0.209
sc22	880		17:56:21.61	-31:05:41.8	-0.6	6.2	0.0030	49.31	994.62	19.910	0.269
sc22	1036		17:57:07.04	-31:04:56.3	-4.2	18.2	0.1727	41.34	592.13	18.904	0.307
sc22	1992	258372	17:56:35.30	-30:56:33.4	-11.0	498.0	0.4108	43.77	944.86	16.972	1.349
sc22	2914	638508	17:57:08.42	-30:48:30.4	-5.8	40.1	0.1457	16.19	1309.04	19.225	0.873
sc22	4328	157685	17:56:21.65	-30:33:27.9	0.0	11.4	0.0346	48.45	694.73	19.038	0.207
sc22	4917	167822	17:56:25.81	-30:26:56.2	-5.1	91.0	0.0959	8.32	1059.36	18.511	1.009
sc23	1334	255351	17:57:40.29	-31:24:27.4	0.2	63.1	0.0977	9.12	635.90	18.908	1.047
sc23	2384	294092	17:57:51.21	-31:10:44.6	-10.2	133.1	0.4499	17.92	1295.53	17.839	0.832
sc23	3833	340296	17:57:41.35	-30:55:33.5	-49.5	220.7	0.3028	36.59	559.38	17.047	0.664
sc23	4183		17:57:42.83	-30:51:51.6	-2.3	22.3	0.1197	11.96	1323.11	18.281	0.206
sc24	429	475158	17:53:51.04	-33:14:05.5	0.1	54.5	0.2576	12.34	608.98	18.376	0.590
sc24	905	198910	17:53:02.79	-33:07:33.4	-27.7	32.1	0.0279	35.18	1287.38	18.991	0.568
sc24	1647		17:53:12.15	-32:56:33.2	-1.3	20.9	0.2266	6.56	654.11	19.043	0.407
sc24	4281		17:53:23.21	-32:25:14.1	-5.0	57.7	0.8744	25.60	565.07	18.911	1.050
sc25	2109		17:54:00.19	-32:40:13.8	1.6	62.5	0.1927	11.57	622.20	18.879	0.990
sc25	2255		17:54:14.47	-32:37:17.4	2.2	567.9	1.0502	12.07	715.11	16.878	1.505
sc26	633		17:46:59.27	-35:18:36.9	-0.8	42.9	0.0643	36.05	1101.56	18.902	0.775
sc26	746	395449	17:47:23.42	-35:17:40.9	1.4	236.6	0.6909	31.28	925.15	17.250	0.883
sc26	1529		17:47:01.50	-35:07:48.9	-2.6	44.9	0.2638	11.61	562.04	18.123	0.358
sc26	2184	85908	17:46:48.16	-34:59:47.2	-20.7	30.8	0.1854	118.48	1400.04	18.004	0.216
sc26	2218		17:47:23.29	-34:59:52.4	-1704.9	2198.9	0.0441	43.36	1331.76	15.075	1.067
sc26	4014		17:47:01.20	-34:41:32.7	-2.2	92.2	0.4663	21.58	713.36	18.343	0.908
sc27	226		17:48:34.11	-35:34:07.0	-4.3	31.9	0.2889	51.36	577.35	18.325	0.306
sc27	759		17:47:54.19	-35:24:36.6	-7.2	39.2	0.4812	22.53	1302.81	20.688	3.500
sc27	946	406020	17:48:36.53	-35:22:58.9	-7.6	29.1	0.1004	42.06	618.94	19.412	0.781
sc27	1438		17:48:16.83	-35:16:24.7	-2.1	0.8	0.0289	288.22	968.38	20.431	0.057
sc27	2790	645326	17:48:55.88	-34:56:13.8	-2.0	40.2	0.1396	49.22	1065.74	19.754	1.623
sc27	3078	331680	17:48:15.92	-34:50:09.0	-10.6	5.6	0.0082	260.82	1243.46	19.442	0.165
sc28	279		17:47:10.54	-37:21:57.4	-9.9	18.9	0.1256	41.89	668.41	20.319	1.104
sc28	695		17:47:31.18	-37:06:39.7	-9.3	8.7	0.1646	47.04	1298.05	19.842	0.363
sc29	281	391055	17:48:35.26	-37:26:49.2	-9.9	37.0	0.4200	14.92	1315.51	18.957	0.716
sc29	303		17:48:13.47	-37:26:11.7	-1.4	414.3	0.8607	7.34	995.27	19.792	16.228
sc29	606		17:48:38.54	-37:20:49.8	-1.8	13.1	0.0953	18.96	608.20	21.224	2.153
sc29	1924		17:48:11.28	-36:48:01.0	-3.7	12.8	0.0847	40.91	640.05	19.738	0.524
sc29	2054	477004	17:48:30.40	-36:45:00.9	-228.9	2097.1	1.2042	63.10	1344.86	14.679	0.768
sc30	1924		18:01:47.68	-29:00:35.7	2.3	14.2	0.0663	67.87	1088.92	18.887	0.239
sc30	1925	631133	18:01:51.72	-29:00:37.7	-15.6	40.2	0.0140	18.74	625.64	18.793	0.622
sc30	1955	57488	18:01:02.52	-29:00:11.6	-82.1	1815.9	0.6735	13.89	1274.79	15.082	0.871
sc30	2475		18:00:57.38	-28:55:13.6	-3.8	16.3	0.0847	33.91	1268.26	18.485	0.184

Table 2—Continued

Field	Star		α_{2000}	δ_{2000}	F_0	F_1	u_0	t_0	$t_{\max}$	I_0	f
	DIA	OGLE									
sc30	2529	471295	18:01:40.20	-28:55:30.4	-14.0	62.3	0.1475	19.92	620.60	18.802	0.953
sc30	3025		18:01:32.71	-28:52:23.9	-3.7	49.8	0.1111	9.89	1410.72	20.181	2.588
sc30	3395	671185	18:01:47.58	-28:49:04.9	-28.5	153.8	0.4136	41.89	557.70	16.052	0.194
sc30	3758	499815	18:01:40.90	-28:46:55.1	-6.5	69.9	0.2318	8.30	1339.02	19.105	1.427
sc30	4491		18:01:44.29	-28:41:30.0	-8.2	117.1	0.5484	31.63	1413.20	18.576	1.495
sc30	5092	145997	18:00:56.67	-28:36:35.9	0.7	116.4	0.0973	18.56	682.15	17.836	0.773
sc30	6124	559419	18:01:33.95	-28:28:02.3	-40.8	3381.1	0.5576	33.93	709.72	14.170	0.774
sc30	6421		18:01:20.13	-28:25:57.3	-3.0	37.8	0.0896	26.96	665.17	19.299	0.880
sc31	537	24931	18:02:00.26	-28:57:27.6	1.1	53.3	0.0722	19.12	930.40	17.598	0.365
sc31	652	631037	18:02:40.11	-28:56:28.2	0.1	9.5	0.0517	89.65	966.39	18.667	0.174
sc31	1076	48308	18:01:58.51	-28:50:08.6	-1.6	513.0	0.8869	8.60	643.96	16.820	1.636
sc31	1795	293442	18:02:22.50	-28:40:43.9	-29.4	6.8	0.0262	32.84	1315.20	18.638	0.108
sc31	2083		18:02:39.57	-28:36:31.3	-29.2	772.0	1.7770	3.19	1349.45	15.350	0.591
sc31	2768	722752	18:02:39.21	-28:29:09.5	-1.1	14.4	0.1004	48.78	605.19	19.039	0.328
sc32	765		18:03:18.81	-28:56:09.2	2.3	8.0	0.0978	45.36	954.01	17.679	0.041
sc32	1336		18:03:53.16	-28:50:13.3	1.3	49.5	0.4438	30.18	699.98	18.318	0.455
sc32	1794		18:03:29.57	-28:44:30.8	2.2	13.2	0.0941	110.09	1445.79	16.381	0.021
sc32	3297	333270	18:03:21.74	-28:28:50.4	3.0	2800.1	0.3600	12.56	1015.81	14.750	1.104
sc33	1997	85552	18:05:02.32	-28:55:17.9	-13.1	51.4	0.0631	64.79	919.27	17.405	0.221
sc33	4090		18:05:45.80	-28:30:52.2	-22.1	7849.7	1.2699	36.84	1546.30	15.214	4.289
sc33	4157		18:05:34.86	-28:30:04.7	-4.5	52.3	0.2170	18.68	1432.58	19.848	1.984
sc34	829		17:58:04.94	-29:29:36.2	-6.7	1897.3	1.9764	29.51	958.30	15.249	1.061
sc34	2535	87132	17:58:00.37	-29:14:59.9	-3.2	23.7	0.0901	33.37	586.10	18.465	0.259
sc34	4692	639703	17:58:22.80	-28:59:54.9	-4.9	26.0	0.0438	62.46	613.62	17.626	0.128
sc34	5241		17:58:41.38	-28:56:28.4	-6.3	36.5	0.3007	64.95	1263.42	17.740	0.208
sc34	7101		17:58:08.63	-28:44:18.2	-39.2	15.8	0.0885	47.66	1352.34	19.810	0.580
sc34	7443		17:58:16.99	-28:42:31.5	-6.5	1271.8	1.2819	57.51	1051.97	15.984	1.425
sc35	166		18:04:15.95	-28:23:10.8	-4.4	70.6	0.6475	41.78	1462.93	18.268	0.648
sc35	1254	54409	18:04:02.88	-28:09:22.4	2.1	47.5	0.0159	35.69	1084.10	17.244	0.164
sc35	1448	451130	18:04:33.63	-28:07:32.2	1.6	2245.1	0.7790	13.82	998.67	15.356	1.451
sc35	1749		18:04:23.68	-28:04:44.0	-23.5	390.1	1.0763	17.30	1347.63	17.855	2.384
sc35	2393		18:04:36.23	-27:59:57.8	-0.5	61.4	0.7801	13.95	634.01	19.718	2.165
sc35	2526	305604	18:04:22.42	-27:57:52.2	-3.8	789.5	1.4136	23.87	688.42	18.905	13.401
sc35	3661		18:04:14.15	-27:46:31.5	-5.1	177.2	1.1161	9.11	1311.73	18.269	1.659
sc35	3812	144974	18:04:09.65	-27:44:34.9	-23.3	906.4	0.5027	31.94	685.02	15.672	0.742
sc35	4208		18:04:29.43	-27:40:45.2	-20.8	35.6	0.3800	76.28	1396.88	18.274	0.336
sc35	5095	770398	18:04:54.02	-27:30:06.8	-18.8	26.0	0.2293	43.80	1301.18	19.649	0.836
sc36	1245		18:05:49.85	-28:17:19.1	-0.9	10.4	0.0312	68.80	706.97	17.933	0.076
sc36	6512		18:05:17.65	-27:43:40.3	-5.4	16.5	0.0546	81.74	1243.34	18.997	0.297
sc36	7980		18:05:16.30	-27:33:55.3	2.2	4.2	0.0240	98.82	648.46	20.279	0.235
sc37	703		17:52:30.48	-30:20:38.1	-2.4	12.2	0.1884	34.47	586.34	19.031	0.230
sc37	1710		17:52:06.36	-30:12:07.1	-3.4	137.8	0.4011	30.42	1003.56	17.565	0.681
sc37	1711		17:52:07.09	-30:12:30.6	-6.0	55.0	0.5717	37.15	1281.80	20.681	4.794
sc37	1864	369822	17:52:36.83	-30:11:30.6	-20.4	2479.5	1.3243	1.97	1316.94	15.232	1.469
sc37	2276		17:52:41.16	-30:08:45.6	-1.4	3.5	0.0735	14.15	631.21	19.479	0.102
sc37	2353		17:52:15.36	-30:08:12.4	-6.5	116.6	0.9810	43.45	993.98	19.433	3.310
sc37	2703	552723	17:52:59.16	-30:06:20.8	-5.3	12.1	0.0655	33.04	629.20	18.527	0.150
sc37	2893	226174	17:52:20.66	-30:04:20.6	-2.4	67.1	0.2138	8.36	557.52	18.481	0.778

Table 2—Continued

Field	Star		α_{2000}	δ_{2000}	F_0	F_1	u_0	t_0	$t_{\max}$	I_0	f
	DIA	OGLE									
sc37	4507	589087	17:52:56.47	-29:54:00.0	-9.2	129.6	0.4222	51.28	692.43	17.460	0.571
sc37	4696	92757	17:52:13.28	-29:52:25.7	-1.8	58.8	0.2420	18.97	689.71	18.125	0.487
sc38	1464	589586	18:01:48.00	-30:09:37.7	-30.7	380.5	1.1862	18.48	1320.21	18.431	3.915
sc38	2547	95103	18:01:09.74	-29:56:18.8	10.6	871.2	0.1524	7.17	990.47	15.990	1.010
sc38	2603	627315	18:01:51.03	-29:56:50.1	-6.5	4973.6	2.3355	13.36	1399.28	16.212	6.693
sc38	3308	120518	18:01:10.23	-29:48:55.2	-337.4	1413.6	0.6919	29.04	1316.14	15.942	1.511
sc39	554		17:55:32.56	-30:08:19.3	-1.3	4.1	0.0436	45.47	604.37	19.072	0.078
sc39	668	442460	17:55:48.70	-30:07:09.6	-4.0	33.9	0.2944	76.98	539.03	19.121	0.695
sc39	1152	448437	17:55:51.90	-30:02:31.4	-25.3	7480.1	1.3760	10.12	1091.72	14.684	2.579
sc39	1235	260832	17:55:23.46	-30:02:09.6	0.2	22.4	0.1278	37.47	652.45	17.974	0.161
sc39	1405	259656	17:55:34.31	-30:01:06.6	-23.4	40.4	0.2675	60.77	1419.79	17.646	0.204
sc39	1794		17:55:19.53	-29:57:57.2	-0.9	1727.3	1.8229	16.38	1218.67	15.515	1.281
sc39	2083		17:55:54.04	-29:56:05.2	-2.7	274.7	0.0605	35.53	508.65	19.695	9.749
sc39	3160	505074	17:55:53.59	-29:47:55.2	-3.6	104.5	0.0217	24.01	1216.07	17.785	0.604
sc39	3613	322789	17:55:26.87	-29:43:59.5	-8.7	1472.1	1.6741	21.16	968.70	15.648	1.189
sc39	3822	323517	17:55:36.42	-29:42:14.0	-2.0	333.5	0.5374	20.03	702.83	16.125	0.454
sc39	3983	702483	17:56:01.60	-29:41:41.6	-2.7	39.6	0.0098	39.08	696.29	18.617	0.511
sc39	5310	362291	17:55:29.29	-29:32:08.7	-54.5	1623.6	1.4829	57.74	1247.84	15.644	1.306
sc39	5900	378193	17:55:30.01	-29:27:38.5	-3.1	3.8	0.0091	162.10	586.73	17.599	0.019
sc40	2433	415182	17:51:14.43	-33:10:31.0	-3.9	39.7	0.0152	19.17	973.03	18.806	0.571
sc40	3640		17:51:16.56	-32:53:44.3	-3.3	4.7	0.0502	154.92	995.71	18.621	0.061
sc41	217		17:52:23.83	-33:31:45.8	-1.3	480.7	0.1516	16.61	700.74	16.653	0.971
sc41	547	172497	17:52:00.69	-33:26:36.2	-6.5	1095.0	1.5860	24.44	684.72	15.889	1.256
sc41	943	345663	17:52:14.52	-33:21:39.0	-2.4	59.2	0.1887	116.52	889.88	17.873	0.385
sc41	1342	353302	17:52:23.56	-33:15:39.1	-10.8	2331.6	2.0056	22.59	548.68	15.266	1.399
sc41	2324	392439	17:52:16.00	-33:02:49.0	2.5	86.1	0.0997	15.94	981.79	17.342	0.331
sc41	2530	402647	17:52:17.00	-33:00:06.5	-8.3	15.7	0.1558	68.04	569.81	20.421	1.054
sc41	2587		17:52:27.08	-32:59:09.9	-18.3	53.8	0.2283	15.40	1374.09	20.123	2.938
sc41	3228		17:51:59.68	-32:49:09.1	-14.4	10.8	0.0643	52.40	1303.35	19.965	0.464
sc41	3299	428823	17:52:19.08	-32:48:20.8	-4.5	61.1	0.2570	49.41	927.31	18.874	0.972
sc42	1089	347998	18:09:10.53	-27:06:42.0	0.3	133.4	0.0061	29.25	1028.29	17.937	0.920
sc42	2633	402431	18:09:20.53	-26:45:47.8	0.5	92.9	0.7133	54.42	1061.17	17.525	0.468
sc42	2761	262259	18:09:04.92	-26:44:38.3	-8.6	7.5	0.0192	51.38	1347.10	17.895	0.047
sc43	225	243401	17:35:13.81	-27:34:38.7	-11.3	550.2	1.1677	16.70	1335.90	17.084	1.714
sc43	416	130624	17:35:07.50	-27:30:37.9	-0.6	296.5	0.4324	14.71	1068.33	17.219	1.047
sc43	836	26773	17:34:52.64	-27:23:14.4	-16.4	148.2	0.4886	65.83	1054.97	17.227	0.536
sc44	1608	17823	17:49:01.67	-30:15:40.4	-29.4	32.4	0.0161	46.12	1392.70	18.884	0.539
sc44	2309	256957	17:49:40.00	-30:10:12.0	-0.8	163.9	0.5865	28.50	1041.39	17.696	1.079
sc44	7582	222903	17:49:22.50	-29:36:52.9	-0.7	63.5	0.0386	12.48	1042.28	19.163	1.318
sc45	492		18:03:15.95	-30:18:42.2	-14.1	399.5	1.2492	11.36	1339.14	18.045	3.834
sc45	1286		18:03:10.88	-29:58:12.9	-27.0	57.6	0.2201	15.53	1314.27	18.451	0.789
sc45	1668		18:03:57.48	-29:51:21.8	-6.2	1140.6	1.4184	15.53	1442.14	15.483	1.093
sc47	1143		17:26:38.93	-39:19:09.5	-35.0	2824.5	2.2374	11.37	1340.35	14.995	1.193
sc48	572		17:28:07.46	-39:44:13.1	-16.2	10.6	0.2057	77.05	1296.46	20.106	0.495
sc48	799		17:28:12.73	-39:26:49.3	0.2	27.5	0.1492	11.13	926.79	20.041	1.180

Table 3. The same as Table 2 for events recovered in the visual search.

Field	Star		α_{2000}	δ_{2000}	F_0	F_1	u_0	t_0	$t_{\max}$	I_0	f
	DIA	OGLE									
sc1	1827		18:02:07.16	-30:02:11.7	-10.0	255.6	1.3514	40.69	1457.39	17.560	1.246
sc1	2096		18:02:24.89	-29:58:44.3	0.2	701.2	1.6048	8.47	1080.94	16.293	1.064
sc1	2411		18:02:42.94	-29:55:02.3	-1.4	17.9	0.1860	9.17	602.82	18.661	0.245
sc1	2624		18:02:45.02	-29:52:59.9	-0.4	97.4	0.8416	2.89	576.66	19.388	2.651
sc1	2948		18:02:11.47	-29:48:24.0	-5.7	53.2	0.4396	31.65	901.67	18.340	0.562
sc1	3087		18:02:38.16	-29:47:44.2	0.3	466.6	1.2134	3.22	967.60	17.474	2.101
sc1	3327		18:02:47.14	-29:44:34.5	-1.4	77.3	0.9806	29.72	602.27	18.129	0.642
sc1	3347		18:03:04.88	-29:45:06.7	-1.2	6.5	0.0201	66.89	636.06	19.663	0.220
sc2	374		18:04:08.83	-29:17:00.5	-79.6	2803.0	1.9919	34.96	1341.38	15.379	1.867
sc2	526		18:04:34.73	-29:16:02.1	-7.5	12.1	0.0704	22.04	1406.65	15.487	0.009
sc2	2011		18:04:32.41	-28:59:02.5	-1.8	1.2	0.0239	111.20	575.29	19.305	0.029
sc2	2035		18:04:44.93	-28:59:24.8	-0.1	358.8	1.2765	7.23	1305.07	16.865	0.957
sc2	2621		18:04:56.11	-28:53:18.5	-5.0	160.8	0.9538	5.18	1395.45	19.024	3.019
sc2	3097		18:04:03.61	-28:47:48.6	-8.1	1868.4	2.6766	52.91	645.79	16.140	2.626
sc2	3130		18:04:38.00	-28:48:03.6	-0.4	51.5	0.0029	89.87	1195.02	17.019	0.157
sc2	4502		18:04:57.54	-28:33:35.6	-8.5	125.3	1.0211	56.23	548.01	18.381	1.363
sc3	247		17:53:21.10	-30:24:13.0	3.2	502.4	1.5188	16.86	1082.87	16.625	1.035
sc3	412		17:54:02.51	-30:23:21.6	1.3	36.4	0.3709	27.99	999.28	19.518	1.098
sc3	2028		17:53:37.57	-30:11:01.1	3.8	13.3	0.2049	36.84	635.42	19.270	0.311
sc3	2729		17:53:14.67	-30:05:43.7	1.0	50.7	0.5804	8.98	697.98	19.789	1.943
sc3	3876		17:53:52.68	-29:58:44.8	-6.3	676.7	1.7081	11.48	1275.74	15.610	0.553
sc3	4000		17:54:06.80	-29:57:12.3	-7.5	7.0	0.1004	42.76	1365.90	20.358	0.434
sc3	4154		17:53:10.50	-29:56:08.8	0.7	41.4	0.4450	10.92	642.53	19.083	0.806
sc3	4761		17:53:41.17	-29:52:00.8	-0.0	18.8	0.1754	8.55	941.00	19.435	0.511
sc3	5027		17:53:46.64	-29:50:06.1	-2.3	58.2	0.5617	11.98	676.89	18.425	0.624
sc3	5815		17:53:11.15	-29:44:42.9	-3.0	75.7	0.7480	23.45	597.74	19.387	1.949
sc3	5852		17:53:33.72	-29:44:48.0	-1.4	121.1	0.7914	5.88	1055.82	17.933	0.781
sc3	5959		17:53:16.21	-29:44:13.0	-6.2	14.0	0.0688	18.49	1336.97	19.661	0.470
sc3	8225		17:54:05.91	-29:32:00.6	-1.0	82.5	0.8095	9.37	951.64	18.781	1.240
sc4	193		17:54:51.02	-30:10:19.4	1.2	5451.8	1.9688	6.18	1097.34	18.239	49.679
sc4	468		17:54:50.90	-30:09:06.0	0.2	77.4	0.6582	5.72	697.12	18.736	1.125
sc4	1904	624085	17:55:00.19	-29:59:53.6	-34.4	1536.7	1.3945	17.49	659.63	15.431	1.093
sc4	2238		17:54:06.80	-29:57:12.2	-0.1	5.3	0.0798	31.77	1366.38	20.124	0.268
sc4	2841		17:54:19.50	-29:54:01.6	-4.3	16.9	0.1865	12.57	1037.84	18.461	0.189
sc4	3598		17:54:07.16	-29:49:29.2	-1.2	42.5	0.5680	18.24	584.83	19.792	1.680
sc4	4561	681764	17:54:55.29	-29:44:38.6	-2.3	95.6	0.3227	21.95	1364.26	18.775	1.454
sc4	5384		17:54:08.07	-29:39:59.7	-6.5	17.7	0.3184	23.58	1050.22	19.028	0.337
sc4	5967		17:54:53.55	-29:36:58.9	-1.1	61.2	0.7397	2.67	631.63	18.007	0.467
sc4	6040		17:54:21.79	-29:36:24.0	-1.2	3.6	0.0465	12.98	963.83	18.949	0.061
sc4	6350		17:54:47.47	-29:34:19.4	-14.7	119.7	1.1026	42.14	1376.09	19.229	2.690
sc4	7404		17:54:36.34	-29:27:13.0	1.2	536.2	0.9269	3.73	945.74	17.990	3.780
sc4	7637		17:54:25.30	-29:25:42.0	1.4	224.0	1.3236	25.84	1284.00	18.561	2.646
sc4	8325		17:54:57.84	-29:21:26.2	-5.2	1644.8	1.8527	45.98	895.79	14.862	0.680
sc4	8361		17:54:12.99	-29:20:00.1	0.4	20.6	0.0368	8.19	1371.39	18.327	0.200
sc4	8468		17:54:16.07	-29:19:05.5	-3.4	7.2	0.0844	21.90	672.48	19.627	0.237
sc4	9035		17:54:22.45	-29:15:48.1	-0.4	7.1	0.0666	56.44	1337.55	16.696	0.016
sc5	1409		17:50:33.78	-30:13:09.3	-2.0	6.6	0.1002	83.60	1297.62	19.377	0.184
sc5	2349		17:50:36.93	-30:06:01.0	-3.4	4.0	0.0415	20.22	1048.74	19.670	0.140

Table 3—Continued

Field	Star		α_{2000}	δ_{2000}	F_0	F_1	u_0	t_0	$t_{\max}$	I_0	f
	DIA	OGLE									
sc5	3634		17:50:27.02	-29:55:12.1	-0.5	171.8	0.7087	0.75	583.46	20.352	12.363
sc5	3789		17:50:48.71	-29:54:41.3	-2.6	11.3	0.0024	13.01	672.55	19.915	0.484
sc5	4301	152125	17:50:13.29	-29:49:57.7	-39.3	759.8	0.0296	169.93	1627.91	15.087	0.370
sc5	4348		17:50:22.52	-29:49:58.7	-8.2	155.7	1.3458	93.75	1313.54	18.469	1.871
sc5	6096		17:50:49.65	-29:38:07.4	-6.9	6.1	0.0009	52.97	1385.70	20.135	0.350
sc5	6129		17:50:05.14	-29:36:54.3	2.6	520.6	1.6706	9.45	968.59	16.562	0.984
sc5	6197		17:50:51.77	-29:36:59.8	-1.1	7.3	0.2075	48.76	563.41	18.988	0.133
sc5	6550		17:50:51.52	-29:34:11.6	-1.5	421.8	1.7413	7.57	613.93	16.177	0.575
sc6	1458		18:07:43.21	-32:07:35.0	-3.1	17.6	0.1601	15.12	1394.65	19.419	0.471
sc6	1592		18:07:46.81	-32:04:20.0	1.8	277.7	1.3169	26.54	943.38	17.325	1.090
sc6	2844		18:08:19.97	-31:44:34.3	-0.6	139.2	0.7876	6.93	1254.23	18.575	1.761
sc7	67		18:09:18.89	-32:32:29.5	2.4	7564.0	2.2510	9.46	750.49	15.604	5.251
sc7	1343		18:08:46.91	-31:47:27.9	-2.4	8.4	0.0828	44.23	1437.66	19.973	0.399
sc7	1492		18:08:42.14	-31:42:34.7	1.2	19.4	0.1607	16.27	1263.06	20.334	1.251
sc8	1184		18:22:41.28	-21:45:24.2	-2.7	97.2	0.3743	4.43	634.47	20.707	7.768
sc8	1243		18:22:51.65	-21:45:06.5	-37.9	3099.8	1.5622	3.42	606.44	19.070	59.588
sc10	2168	220492	18:20:06.49	-22:03:58.6	-76.6	246.5	0.6944	103.49	584.71	17.499	1.157
sc11	446		18:21:09.33	-22:41:32.7	-0.8	514.6	1.7072	4.19	1290.48	19.354	12.855
sc12	998		18:15:59.02	-24:10:04.8	-10.4	0.5	0.0022	244.19	1397.29	19.605	0.015
sc12	1900		18:16:26.45	-23:56:00.6	-6.8	0.2	0.0003	1441.86	1086.42	18.300	0.002
sc12	2964		18:15:42.58	-23:38:18.6	-0.7	63.4	0.7663	4.09	656.95	20.629	5.083
sc13	51		18:16:44.62	-24:24:13.7	-0.4	42.9	0.3895	3.00	630.59	19.609	1.616
sc14	86		17:46:49.01	-23:34:14.6	-1.7	75.4	0.5505	8.14	944.45	19.198	1.558
sc14	587		17:47:32.94	-23:27:23.9	-23.2	13157	2.3662	2.91	603.59	20.814	1321.0
sc14	1036	508950	17:47:20.67	-23:20:08.7	-1.4	81.6	0.0211	109.67	804.38	17.823	0.516
sc14	2847		17:46:52.59	-22:58:12.6	-1.0	56.2	0.4106	10.99	972.91	20.231	3.091
sc15	473	20039	17:47:37.21	-23:27:03.0	-5.8	210.2	0.0214	43.59	674.94	17.474	0.888
sc15	979		17:48:20.13	-23:19:58.2	-4.0	11.9	0.1381	42.63	1375.82	20.108	0.588
sc15	1631	373196	17:48:07.05	-23:12:03.2	-10.2	7.0	0.00004	12.52	573.04	19.527	0.197
sc16	365		18:10:17.16	-26:41:10.0	0.6	45.8	0.1298	17.21	962.61	20.405	2.959
sc16	673		18:10:15.52	-26:37:48.7	-1.6	245.9	0.0747	20.24	875.64	17.823	1.485
sc16	1017		18:10:17.66	-26:33:45.3	2.4	877.4	1.5253	4.93	959.60	16.420	1.497
sc16	1048	32304	18:09:38.47	-26:32:26.8	-21.4	13.3	0.0186	32.77	573.73	18.422	0.141
sc16	3507		18:10:18.30	-26:04:59.6	-7.2	52.4	0.7782	40.98	1309.58	19.145	1.041
sc16	3633		18:10:05.06	-26:03:47.8	-6.5	75.2	0.6025	25.34	1459.88	18.788	1.026
sc17	159		18:11:21.83	-26:38:11.6	-0.3	36.1	0.1441	12.91	1047.47	19.055	0.731
sc17	2199	270411	18:10:59.48	-26:13:16.7	-1.2	70.4	0.3818	18.12	1043.23	18.402	0.766
sc17	4042		18:11:00.95	-25:50:46.1	-1.4	350.1	1.8024	21.06	909.11	20.233	19.659
sc18	165	579405	18:07:21.01	-27:40:04.0	-4.4	9.7	0.0911	184.68	1472.48	16.571	0.020
sc18	485		18:07:10.97	-27:36:35.5	-0.9	289.5	1.3279	3.58	549.03	18.667	3.804
sc18	844	424029	18:07:05.62	-27:32:39.3	-8.4	21.8	0.3047	25.61	1358.69	18.311	0.212
sc18	1136		18:06:55.65	-27:29:08.8	-1.8	201.9	1.0022	7.06	1293.74	17.910	1.250
sc18	2757		18:07:29.75	-27:14:52.3	2.8	426.4	0.9865	15.05	1115.27	17.069	1.298
sc18	4591		18:07:32.39	-26:57:37.5	-7.6	1436.3	2.3609	3.03	1349.51	17.099	4.580
sc18	4924		18:06:54.66	-26:54:02.8	-7.0	318.1	1.4558	40.98	1261.50	18.541	3.829
sc19	669	26606	18:07:45.14	-27:33:15.2	-195.0	40.5	0.0309	47.93	1346.94	17.868	0.269
sc19	713		18:07:57.21	-27:33:28.8	-13.0	6054.6	2.0248	3.83	1312.46	20.562	423.40
sc19	1462		18:07:36.33	-27:24:28.0	-1.3	298.1	0.9559	5.58	1065.92	15.494	0.198

Table 3—Continued

Field	Star		α_{2000}	δ_{2000}	F_0	F_1	u_0	t_0	$t_{\max}$	I_0	f
	DIA	OGLE									
sc19	2494		18:07:52.91	-27:13:55.6	-2.8	48.6	0.5341	11.67	1299.13	19.056	0.864
sc19	3090		18:08:04.10	-27:06:54.7	-5.7	165.9	1.1592	30.55	1265.30	18.189	1.293
sc19	3710		18:07:43.03	-27:00:12.8	-17.6	756.8	1.3305	3.83	1351.39	>20.5	?
sc19	3964		18:07:45.51	-26:57:10.2	-3.5	554.0	1.0638	4.56	1061.48	18.029	3.866
sc19	4328		18:07:45.29	-26:53:21.9	-6.2	3.4	0.0876	150.05	630.36	18.781	0.047
sc20	337		17:59:04.67	-29:17:03.4	-9.8	1455.2	0.7154	2.61	955.67	15.807	1.348
sc20	594		17:58:54.90	-29:14:52.5	-4.5	36.0	0.1117	38.61	1098.52	18.702	0.484
sc20	1436		17:59:37.27	-29:07:54.9	-10.8	0.2	0.0031	397.17	1365.44	20.084	0.010
sc20	1767		17:59:37.66	-29:04:09.0	5.0	548.9	1.6522	34.24	1031.24	16.415	0.866
sc20	2825		17:58:49.55	-28:53:16.1	0.7	132.4	1.0323	30.93	641.42	18.336	1.181
sc20	3780		17:58:47.13	-28:44:50.4	-2.0	2.0	0.0168	282.50	1101.16	19.025	0.038
sc20	3912		17:59:17.22	-28:43:30.0	-16.6	4712.1	2.5698	6.20	654.21	14.140	0.966
sc20	4695		17:59:14.40	-28:36:55.6	-2.0	0.1	0.0009	2727.35	580.40	19.083	0.001
sc20	5229		17:59:01.56	-28:31:28.1	-0.3	2.5	0.0118	70.80	963.47	18.435	0.026
sc20	5875	395103	17:59:08.99	-28:24:54.7	-184.2	1758.5	0.3810	32.44	947.25	15.513	1.375
sc21	1355		18:00:39.55	-29:10:11.7	-1.9	54.5	0.5752	9.56	585.16	19.275	1.253
sc21	2195		17:59:58.88	-29:02:25.3	0.5	66.3	0.6124	59.76	714.00	18.514	0.778
sc21	2719		18:00:17.43	-28:59:07.6	-0.9	10.9	0.2175	198.77	1077.82	18.891	0.168
sc21	3929		18:00:49.25	-28:51:38.0	-0.1	1053.8	0.5429	2.30	671.29	17.227	3.677
sc21	6195	833776	18:00:39.58	-28:34:43.3	-7.3	0.8	0.0018	1680.15	592.21	17.721	0.004
sc21	6389		18:00:36.13	-28:32:34.6	-1.8	292.4	0.8159	16.17	531.44	16.304	0.420
sc21	6417		18:00:48.47	-28:32:48.1	-4.5	219.6	1.1934	10.22	1393.41	18.472	2.325
sc22	1096		17:56:39.34	-31:04:18.3	10.0	253.9	0.2413	17.45	636.48	15.687	0.215
sc22	1840		17:57:10.84	-30:57:30.1	-1.5	58.7	0.8722	17.25	1226.37	18.993	1.013
sc22	1958		17:56:25.16	-30:55:50.8	-6.4	128.3	0.0847	15.95	539.19	18.146	1.034
sc22	2467		17:56:33.88	-30:51:31.1	-5.8	10.5	0.1300	15.77	554.10	19.883	0.417
sc22	2644		17:56:19.97	-30:49:52.7	-7.1	703.4	1.2407	87.49	439.17	17.670	3.691
sc22	3735		17:57:12.47	-30:40:32.2	0.7	44.1	0.2786	10.28	638.15	19.356	1.064
sc22	4692		17:56:42.84	-30:29:44.4	2.4	789.5	1.7154	4.95	1030.45	16.258	1.048
sc23	294		17:57:29.38	-31:37:10.4	-0.3	96.1	0.6386	6.92	1440.95	20.178	4.988
sc23	1254		17:57:22.33	-31:25:32.3	-8.3	3763.8	0.1557	1.00	1043.87	19.796	145.26
sc23	1379		17:57:27.32	-31:23:55.3	-0.9	130.3	0.6559	7.22	968.96	19.159	2.771
sc23	2041	282632	17:57:46.55	-31:14:28.2	-1.9	2174.8	2.2286	1.80	632.89	17.655	11.467
sc24	374		17:52:53.52	-33:14:00.1	-3.0	157.3	1.4866	43.34	627.31	17.546	0.750
sc24	1212		17:53:06.33	-33:03:09.4	-3.1	3.6	0.0624	21.94	665.31	20.061	0.165
sc24	1409		17:53:17.69	-33:00:17.5	-2.6	46.3	0.4446	6.81	965.24	19.248	1.010
sc24	1453	57233	17:52:53.01	-32:59:02.3	-3.8	669.6	1.5093	35.30	1019.42	16.462	1.155
sc24	2403		17:52:53.32	-32:45:45.8	-2.1	15.1	0.2293	21.54	650.35	20.162	0.781
sc24	2414		17:53:02.52	-32:46:09.2	-1.1	298.3	1.3027	13.42	921.11	17.241	1.055
sc24	3042	111303	17:52:56.51	-32:38:51.3	0.2	249.1	0.9838	13.62	542.12	18.058	1.834
sc24	3377	137412	17:52:54.69	-32:34:44.4	-2.6	15.4	0.1813	117.19	1067.62	19.236	0.333
sc24	4060		17:53:20.84	-32:27:48.4	-3.5	63.0	0.7820	14.26	949.22	18.287	0.600
sc25	888		17:54:34.50	-33:02:56.8	-3.1	66.2	0.6112	2.77	673.39	18.677	0.862
sc25	1364		17:54:10.38	-32:53:19.3	0.2	85.2	0.9526	2.67	671.23	19.912	3.397
sc25	1584		17:54:03.28	-32:48:38.5	-18.6	16.3	0.0843	26.93	1279.94	19.187	0.342
sc26	655		17:47:20.17	-35:18:38.1	-3.4	161.4	1.2855	26.28	580.68	17.199	0.554
sc26	2165		17:47:36.63	-35:00:41.7	-1.7	256.2	0.8838	16.68	1110.67	18.538	3.075
sc26	2232		17:47:23.20	-34:59:57.0	-2.9	38.1	0.2403	12.15	1330.87	18.178	0.322

Table 3—Continued

Field	Star DIA	Star OGLE	α_{2000}	δ_{2000}	F_0	F_1	u_0	t_0	$t_{\max}$	I_0	f
sc27	570	23935	17:47:57.58	-35:27:20.6	-4.7	677.1	1.1324	14.86	886.68	16.656	1.462
sc27	899		17:48:41.41	-35:23:45.0	-4.4	0.2	0.0043	639.72	1367.28	19.481	0.005
sc27	1510		17:48:27.78	-35:15:23.9	-0.9	237.5	1.5197	18.48	673.55	19.627	7.627
sc27	1928		17:48:00.62	-35:08:17.8	-3.8	1.1	0.0223	67.68	1317.20	19.533	0.038
sc28	547		17:47:26.54	-37:12:00.6	-0.1	0.8	0.0002	80.41	571.37	19.321	0.019
sc28	936		17:46:34.88	-36:57:55.1	2.9	614.1	1.7683	18.74	964.70	16.151	0.788
sc28	1159		17:47:17.06	-36:51:49.7	-3.3	629.3	1.6895	2.68	1290.98	21.698	136.21
sc28	1395		17:46:47.37	-36:41:47.4	-14.6	33.4	0.1077	6.73	1322.32	19.190	0.718
sc30	1272	236837	18:01:18.13	-29:05:50.0	2.5	6.5	0.0003	474.29	908.42	17.002	0.019
sc30	1469		18:01:12.22	-29:04:14.5	2.4	1422.3	1.6293	5.33	959.35	16.534	2.772
sc30	1782		18:01:15.01	-29:01:48.3	-1.0	100.1	0.1640	5.73	672.00	18.123	0.820
sc30	1923		18:01:47.30	-29:00:41.2	-6.0	523.0	1.8036	6.88	1348.42	16.418	0.907
sc30	2320		18:01:32.30	-28:57:49.1	-3.0	180.1	1.2264	8.04	1406.58	18.245	1.620
sc30	2628		18:01:32.67	-28:54:45.9	-2.8	724.6	1.8061	26.72	650.66	16.084	0.883
sc30	3977		18:01:18.59	-28:45:02.0	-8.6	243.6	1.4193	41.34	586.11	17.458	1.033
sc30	4398		18:00:55.72	-28:41:26.4	-1.4	160.6	0.6295	5.96	1081.14	18.662	2.219
sc30	5369		18:01:27.19	-28:34:45.7	-4.1	181.2	1.0661	10.13	614.05	18.447	2.018
sc30	5706		18:01:21.50	-28:31:24.5	3.1	254.1	0.8560	54.75	809.43	17.284	0.979
sc30	5854		18:01:52.83	-28:30:43.6	-4.0	49.6	0.7240	4.45	1291.30	17.984	0.367
sc30	5983		18:01:05.50	-28:29:26.1	-1.6	68.1	0.5309	22.07	1094.32	18.149	0.582
sc30	6563		18:01:38.06	-28:24:31.3	-2.9	755.1	1.5014	4.11	1333.33	16.895	1.977
sc31	288		18:01:51.72	-29:00:37.7	-5.3	102.7	0.6248	13.87	625.90	18.712	2.073
sc31	538		18:02:02.32	-28:57:07.7	1.1	564.8	1.8151	24.52	624.82	16.984	2.196
sc31	1915		18:02:11.81	-28:38:48.6	-1.6	138.2	0.5870	11.13	1099.19	18.726	2.264
sc31	2369		18:02:44.30	-28:33:09.0	0.4	17.1	0.0956	17.29	1257.06	18.145	0.166
sc31	3094	342145	18:02:17.96	-28:25:28.2	-14.1	302.3	1.3259	6.78	1344.18	16.557	0.630
sc31	3205		18:02:17.56	-28:24:10.1	-19.3	10.1	0.0701	36.24	1321.07	19.643	0.354
sc31	3614		18:02:43.53	-28:20:49.2	-66.0	3074.6	2.2863	16.33	1303.59	13.945	0.573
sc32	349		18:03:28.61	-29:01:30.8	-1.3	107.3	0.7298	1.34	1367.16	18.271	0.944
sc32	2250		18:03:07.13	-28:39:10.5	-0.1	16.6	0.0893	7.52	634.70	18.439	0.187
sc32	2755		18:03:12.41	-28:35:02.3	-46.5	324.0	1.1851	45.63	1311.31	17.563	1.659
sc32	3480	737024	18:03:45.40	-28:27:13.1	4.8	702.6	0.0542	37.45	832.03	16.538	1.337
sc32	4302		18:02:55.89	-28:16:56.3	-0.8	251.9	0.4727	5.59	571.46	17.727	1.486
sc32	4683		18:02:57.13	-28:12:53.3	-18.3	276.5	1.3661	29.65	1295.82	17.241	1.072
sc32	5005		18:03:55.36	-28:09:59.2	-2.5	61.3	0.2799	37.87	1223.95	18.155	0.546
sc33	1749		18:05:46.82	-28:58:19.5	-2.0	189.2	1.2912	15.97	1262.35	19.076	3.626
sc33	3423		18:05:18.48	-28:39:57.6	-13.5	150.9	0.7678	10.39	1291.26	20.328	9.333
sc33	4505	553617	18:05:46.71	-28:25:32.1	-172.0	756.9	0.4188	162.63	648.03	15.742	0.660
sc34	249		17:58:03.08	-29:33:46.7	-5.9	63.9	0.6754	62.62	1458.05	17.967	0.425
sc34	600		17:57:55.47	-29:31:26.8	-0.9	213.4	1.1014	23.50	1465.63	18.726	3.018
sc34	644		17:58:25.10	-29:30:51.5	-0.0	486.0	1.4948	2.92	630.78	17.670	2.598
sc34	1570		17:58:16.31	-29:23:22.5	-3.3	1131.7	1.8760	3.50	554.52	15.505	0.832
sc34	2091		17:57:58.63	-29:18:54.3	-5.1	210.6	0.9321	4.64	550.96	17.611	1.019
sc34	2372		17:58:25.50	-29:17:22.2	-0.5	15.9	0.1082	33.52	1449.96	15.327	0.010
sc34	2783		17:58:03.07	-29:13:41.6	-16.9	8189.6	2.5462	15.07	522.43	14.346	1.922
sc34	3332		17:58:18.94	-29:09:51.4	-0.2	3.4	0.0702	90.56	1049.34	18.723	0.046
sc34	3901		17:58:34.18	-29:06:29.6	-1.4	1510.0	1.8512	18.17	975.32	15.268	0.859
sc34	3906	840343	17:58:37.11	-29:06:29.9	-93.8	28054.8	0.8827	49.21	798.82	13.602	3.443

Table 3—Continued

Field	Star		α_{2000}	δ_{2000}	F_0	F_1	u_0	t_0	$t_{\max}$	I_0	f
	DIA	OGLE									
sc34	4122		17:58:25.05	-29:04:38.4	-1.6	212.5	0.9541	4.68	1297.83	18.003	1.530
sc34	4172	144644	17:57:47.60	-29:03:54.3	-3.6	469.4	0.1954	9.93	949.44	16.377	0.695
sc34	4503		17:58:00.36	-29:00:59.5	-6.1	20.8	0.2689	10.78	561.91	18.810	0.296
sc34	4536		17:58:15.40	-29:01:38.0	-1.2	80.8	0.0264	24.40	878.68	17.236	0.276
sc34	4694		17:58:31.20	-29:00:18.2	-9.4	17.3	0.0101	101.65	532.89	18.049	0.125
sc34	4695		17:58:33.83	-29:00:04.0	0.9	71.8	0.5668	6.79	1288.15	20.048	3.276
sc34	5397		17:58:36.25	-28:56:16.5	-0.1	92.7	0.7763	13.63	638.24	18.849	1.442
sc34	5590		17:57:55.78	-28:54:05.7	1.2	9.6	0.1348	14.24	634.18	19.692	0.317
sc35	226		18:04:06.99	-28:22:18.4	-9.3	15.3	0.1675	37.49	1291.87	18.082	0.126
sc35	2854		18:04:01.24	-27:54:57.9	-4.1	297.8	0.9687	9.91	954.42	18.335	3.048
sc35	4923		18:04:29.34	-27:31:31.4	-3.0	23.1	0.1292	15.56	1242.04	19.022	0.421
sc35	5003		18:04:37.20	-27:31:05.0	-61.4	1641.5	1.9080	68.33	1295.61	15.260	0.980
sc36	343		18:05:36.77	-28:23:10.2	-11.3	756.5	1.1073	1.70	1396.83	16.092	1.046
sc36	1869		18:05:26.53	-28:12:37.7	-0.8	312.1	1.4596	28.57	670.56	17.197	1.069
sc36	2209		18:05:07.19	-28:10:12.4	-17.9	25.8	0.0493	7.73	1298.95	18.749	0.362
sc36	4030	336761	18:05:29.59	-27:59:14.3	-46.1	4.2	0.0399	273.95	1304.70	18.537	0.051
sc36	4057		18:05:38.59	-27:59:19.1	-4.6	120.0	1.1152	7.56	1322.18	18.094	0.984
sc36	6759		18:05:02.47	-27:42:16.6	-2.6	406.9	1.4043	136.04	567.60	18.129	3.321
sc37	560		17:52:14.38	-30:21:31.0	-2.1	35.3	0.5164	22.60	1340.51	19.160	0.772
sc37	2277		17:52:41.69	-30:08:28.5	-4.8	249.1	1.3070	6.00	940.26	19.826	9.880
sc37	2800		17:52:32.90	-30:05:20.2	3.2	295.9	1.4639	18.51	681.10	16.639	0.647
sc37	2803		17:52:38.99	-30:05:28.1	-0.6	260.9	1.4280	4.17	560.20	17.658	1.458
sc37	3241		17:52:10.99	-30:01:18.4	-1.6	19.7	0.1845	118.87	520.18	18.945	0.361
sc37	3289		17:52:36.89	-30:01:54.2	-0.3	5.7	0.0501	19.14	611.21	19.693	0.197
sc37	3639		17:52:46.37	-29:59:03.4	0.5	338.1	1.1405	3.57	599.74	20.032	16.357
sc37	4438		17:52:20.46	-29:53:43.8	-5.1	13.1	0.1765	20.72	663.67	19.989	0.587
sc37	5284		17:52:37.86	-29:48:16.1	-0.8	166.7	1.0191	3.16	1365.94	17.642	0.853
sc37	5734		17:52:22.88	-29:44:39.8	-5.1	26.7	0.2288	8.76	1416.56	20.031	1.291
sc37	5772		17:52:36.27	-29:45:15.0	-2.7	10.0	0.1737	16.84	1339.52	19.477	0.290
sc37	6075		17:52:02.34	-29:42:39.4	-4.4	76.6	0.3093	4.25	1063.09	18.777	1.212
sc37	6360		17:52:30.17	-29:40:18.4	-0.8	4.7	0.0638	49.12	1343.32	16.266	0.007
sc37	7600		17:52:45.02	-29:33:24.2	-7.4	176.7	1.1704	9.03	702.39	18.476	2.022
sc38	224		18:01:06.74	-30:22:18.6	-1.0	446.7	1.5866	6.71	963.02	17.653	2.371
sc38	749		18:01:16.84	-30:17:04.3	-2.0	2.8	0.0185	99.82	1255.10	18.685	0.036
sc38	2298	447654	18:01:34.42	-30:00:07.7	-14.8	136.2	0.7194	76.40	555.16	17.331	0.514
sc38	3314		18:01:02.95	-29:48:39.1	-13.1	65.5	0.0381	15.69	1064.49	18.052	0.489
sc38	3465		18:01:11.39	-29:46:54.4	-3.5	19.3	0.0994	33.45	1248.59	17.918	0.129
sc39	512	623258	17:56:04.05	-30:08:53.1	-11.7	500.9	0.9318	72.68	1169.55	16.926	1.362
sc39	1179		17:55:58.21	-30:03:06.6	-4.6	44.8	0.7443	4.88	571.52	19.275	1.101
sc39	1271		17:55:50.15	-30:01:49.7	-1.4	26.2	0.4066	14.74	936.70	20.344	1.678
sc39	1969	468687	17:55:45.16	-29:56:38.7	-3.1	1535.0	1.7994	36.28	1209.73	15.825	1.513
sc39	3221		17:55:19.61	-29:47:05.4	2.2	7.8	0.0527	31.63	1239.84	18.658	0.101
sc39	3550		17:55:55.57	-29:45:17.7	-2.8	41.2	0.1434	9.57	962.16	18.518	0.481
sc39	3666		17:56:10.58	-29:44:31.7	-10.3	954.2	1.4982	10.02	1422.10	16.413	1.588
sc39	5030	729484	17:55:56.71	-29:35:01.0	-6.6	84.8	0.6919	93.68	647.53	19.556	2.721
sc39	5336		17:55:50.86	-29:31:43.7	0.9	15.5	0.1237	11.89	1066.68	18.265	0.147
sc39	6303		17:56:00.99	-29:25:11.9	-6.9	2203.7	2.1828	8.97	1242.52	14.962	0.972
sc39	6407	576039	17:55:43.97	-29:24:28.5	-7.7	707.0	1.6892	38.03	619.49	16.022	0.860

Table 3—Continued

Field	Star		α_{2000}	δ_{2000}	F_0	F_1	u_0	t_0	$t_{\max}$	I_0	f
	DIA	OGLE									
sc39	7091		17:55:40.83	-29:19:05.7	-0.2	16.9	0.1451	19.32	1070.42	17.030	0.053
sc40	642	497858	17:51:31.82	-33:34:00.8	-30.1	49.0	0.1283	15.68	1323.13	17.650	0.267
sc40	955		17:50:57.73	-33:28:50.1	-0.3	329.5	1.5152	17.84	699.72	19.418	8.109
sc40	1005	40759	17:50:43.81	-33:27:47.6	-5.2	3460.9	2.3196	1.92	1309.16	16.800	8.229
sc40	1796		17:50:46.06	-33:18:32.5	-1.9	233.3	1.0827	7.59	1440.00	18.800	3.403
sc40	2644		17:50:34.16	-33:06:56.9	-7.0	8.9	0.1148	165.93	949.30	20.247	0.491
sc40	2658		17:50:51.05	-33:07:02.1	-0.9	50.9	0.7221	26.33	630.27	18.534	0.597
sc40	2757		17:51:07.26	-33:06:10.8	0.4	389.2	1.4486	2.96	582.86	18.894	6.304
sc40	2868	574713	17:51:31.65	-33:04:51.0	-0.9	7695.8	0.0118	3.63	544.59	17.286	29.419
sc40	2869	573818	17:51:31.79	-33:04:42.0	-23.9	1742.9	1.4474	43.34	528.92	15.230	1.003
sc40	2918		17:51:32.54	-33:04:02.0	-1.7	9.9	0.0927	34.71	1401.16	19.509	0.288
sc41	1784		17:52:06.22	-33:10:38.2	-4.4	125.8	1.0216	38.79	540.46	18.198	1.034
sc41	1975		17:52:17.16	-33:08:10.4	-1.7	344.2	0.6586	6.76	991.61	17.362	1.398
sc41	2354		17:51:37.04	-33:01:46.7	-8.3	46.5	0.7563	21.95	1348.61	19.386	1.229
sc41	2607	100122	17:51:42.96	-32:58:19.0	-1.2	266.2	1.2074	36.24	1054.71	17.306	1.066
sc41	3208	568646	17:52:31.53	-32:50:52.8	4.1	102.0	0.4818	46.59	1123.14	17.929	0.732
sc42	453		18:09:30.76	-27:14:49.0	-18.9	1.6	0.0029	239.08	1353.38	18.824	0.026
sc42	510		18:09:18.66	-27:13:26.2	-2.5	19.9	0.0186	12.70	1444.06	19.248	0.450
sc42	3851		18:08:36.68	-26:30:14.0	-0.6	981.3	1.4898	3.03	629.71	19.082	19.978
sc43	103		17:35:00.55	-27:36:20.7	-1.5	360.9	1.3042	6.10	614.80	19.199	7.533
sc43	1595		17:34:53.59	-27:12:24.8	-1.1	42.5	0.6321	10.22	940.71	18.173	0.385
sc43	2416		17:35:20.15	-27:00:05.6	3.6	492.7	1.5214	9.82	1397.77	16.297	0.730
sc43	2482	319475	17:35:24.56	-26:59:28.2	3.2	200.7	0.7113	7.44	976.49	17.227	0.700
sc43	2861		17:34:53.53	-26:52:22.6	-31.5	2945.1	0.9968	3.75	1421.35	14.982	1.361
sc44	45		17:49:13.01	-30:30:38.1	-1.4	43.9	0.0990	3.52	609.50	20.464	3.282
sc44	1910		17:49:10.46	-30:13:02.8	-7.6	55.6	0.7155	121.99	731.67	18.820	0.906
sc44	5711	288419	17:49:49.13	-29:49:10.4	6.7	84.1	0.2286	17.96	967.32	16.798	0.213
sc44	6977		17:49:29.70	-29:41:22.7	-3.7	45.9	0.6531	19.02	662.96	19.429	1.286
sc45	141		18:03:14.11	-30:28:06.5	-5.6	311.0	1.4293	29.18	1231.51	17.087	1.223
sc45	180		18:04:00.26	-30:28:34.6	-8.5	184.2	0.6143	47.09	954.20	17.243	0.926
sc45	810		18:03:30.06	-30:09:55.6	-1.6	816.9	1.2425	25.35	693.66	17.493	4.937
sc45	1695		18:03:34.35	-29:50:42.8	-9.5	440.7	1.2664	11.49	1269.37	16.571	1.058
sc46	784		18:04:13.50	-30:09:25.5	0.6	7891.1	0.0669	33.94	578.37	15.484	7.222
sc49	614		17:29:07.69	-40:05:21.4	-0.5	38.4	0.5058	9.60	987.66	21.257	5.331
sc49	691		17:28:49.54	-39:57:57.6	-3.5	46.6	0.8656	16.67	1398.22	20.661	3.703

Table 4. The same as Table 2 for additional microlensing events recovered through cross identification with the OGLE catalog.

Field	Star		α_{2000}	δ_{2000}	F_0	F_1	u_0	t_0	$t_{\max}$	I_0	f
	DIA	OGLE									
sc3	7783	590098	17:53:47.68	-29:34:45.1	-2.8	13898.2	2.6588	2.17	579.35	17.293	50.614
sc5	2859	244353	17:50:36.09	-30:01:46.6	-320.1	377.8	0.0894	248.33	529.46	18.351	3.934
sc5	4321	152125	17:50:13.29	-29:49:56.9	-15.7	2084.6	0.0568	68.13	1580.15	15.075	0.998
sc33	3764	164492	18:05:05.35	-28:34:42.5	-229.7	31.2	0.0231	648.86	1365.66	18.093	0.241
sc37	8176	321846	17:52:20.49	-29:31:15.4	-1.2	702.4	1.7315	26.30	530.49	17.043	2.107
sc40	2895	434222	17:51:10.76	-33:03:44.1	-175.0	79.9	0.2204	435.88	1326.99	16.060	0.092
sc44	1980	20145	17:48:56.53	-30:11:40.8	-205.6	1219.0	0.7573	89.54	607.03	15.837	1.194
sc44	2050	172247	17:49:33.12	-30:11:56.1	-6.3	228.1	1.3794	48.98	1360.95	17.874	1.536


This figure "wozniak.fig4a.gif" is available in "gif" format from:
http://arXiv.org/ps/astro-ph/0106474v1

This figure "wozniak.fig4b.gif" is available in "gif" format from:

http://arXiv.org/ps/astro-ph/0106474v1


This figure "wozniak.fig4c.gif" is available in "gif" format from:
http://arXiv.org/ps/astro-ph/0106474v1

This figure "wozniak.fig4d.gif" is available in "gif" format from:

http://arXiv.org/ps/astro-ph/0106474v1


This figure "wozniak.fig4e.gif" is available in "gif" format from:
http://arXiv.org/ps/astro-ph/0106474v1


This figure "wozniak.fig4f.gif" is available in "gif" format from:
http://arXiv.org/ps/astro-ph/0106474v1

This figure "wozniak.fig4g.gif" is available in "gif" format from:

http://arXiv.org/ps/astro-ph/0106474v1

This figure "wozniak.fig4h.gif" is available in "gif" format from:

http://arXiv.org/ps/astro-ph/0106474v1


This figure "wozniak.fig5a.gif" is available in "gif" format from:
http://arXiv.org/ps/astro-ph/0106474v1


This figure "wozniak.fig5b.gif" is available in "gif" format from:
http://arXiv.org/ps/astro-ph/0106474v1


This figure "wozniak.fig5c.gif" is available in "gif" format from:
http://arXiv.org/ps/astro-ph/0106474v1


This figure "wozniak.fig5d.gif" is available in "gif" format from:
http://arXiv.org/ps/astro-ph/0106474v1

This figure "wozniak.fig5e.gif" is available in "gif" format from:

http://arXiv.org/ps/astro-ph/0106474v1

This figure "wozniak.fig5f.gif" is available in "gif" format from:

http://arXiv.org/ps/astro-ph/0106474v1


This figure "wozniak.fig5g.gif" is available in "gif" format from:
http://arXiv.org/ps/astro-ph/0106474v1

This figure "wozniak.fig5h.gif" is available in "gif" format from:

http://arXiv.org/ps/astro-ph/0106474v1


This figure "wozniak.fig5i.gif" is available in "gif" format from:
http://arXiv.org/ps/astro-ph/0106474v1


This figure "wozniak.fig6.gif" is available in "gif" format from:
http://arXiv.org/ps/astro-ph/0106474v1